Technical Note

1976-18

J. T. Mayhan

Adaptive Nulling with Multiple-Beam Antennas

30 September 1976

Prepared for the Defense Communications Agency
under Electronic Systems Division Contract F19628-76-C-0002 by

Lincoln Laboratory
MASSACHUSETTS INSTITUTE OF TECHNOLOGY
LEXINGTON, MASSACHUSETTS

The work reported in this document was performed at Lincoln Laboratory, a center for research operated by Massachusetts Institute of Technology, for the Military Satellite Office of the Defense Communications Agency under Air Force Contract F19628-76-C-0002.

This technical report has been reviewed and is approved for publication.

FOR THE COMMANDER

Raymond L. Loiselle, Lt. Col., USAF
Chief, ESD Lincoln Laboratory Project Office

MASSACHUSETTS INSTITUTE OF TECHNOLOGY
LINCOLN LABORATORY

ADAPTIVE NULLING WITH MULTIPLE-BEAM ANTENNAS

J. T. MAYHAN
Group 61

TECHNICAL NOTE 1976-18

30 SEPTEMBER 1976

LEXINGTON MASSACHUSETTS

ABSTRACT

This technical note discusses some of the more prominent features of an Applebaum-Howells type adaptive nulling algorithm when used in conjunction with a multiple-beam antenna operating over the earth field of view at synchronous altitude. A brief discussion of some of the basic properties of the multiple-beam antenna configuration used in the study is presented, following which some of the characteristics of the conventional LMS power minimization algorithm, such as the Applebaum-Howells type, as they apply to the multiple-beam antenna are developed. The relationship of the adapted radiation pattern to radiation pattern synthesis techniques is discussed. Next the time required for the algorithm to adapt to the steady state solution is considered. For the LMS algorithm, the dynamic range of interference power levels to be nulled sets the dynamic range of adaption times required by the adaptive algorithm. This spread in adaption times is related to the spread in the eigenvalues of the interfering-source correlation matrix defined at the receive ports. Techniques for compressing this eigenvalue spread, and hence increasing the dynamic range of the algorithm, are determined.

CONTENTS

Adaptive Nulling with Multiple-Beam Antennas

I. Introduction

This technical note discusses some of the more prominent features of an Applebaum-Howells type adaptive nulling algorithm when used in conjunction with a multiple-beam antenna (MBA), operating over the earth field of view (FOV) at synchronous altitude. Several variations of the Applebaum-Howells algorithm have been implemented in practice. The particular variation we adopt is essentially that discussed by Gabriel.[1] This scheme allows for the incorporation of "beam steering" weights into the control loops, which govern the behavior of the adapted radiation pattern. Incorporation of this scheme with a multiple-beam antenna allows for the use of a large aperture in order to obtain pattern shaping capabilities over a limited FOV, while keeping the number of signal ports at a tractable number.

A parameter of particular interest in evaluating the usefulness of most adaptive nulling algorithms is the time required for adaption to take place. One of the basic limitations to the use of a conventional LMS power minimization algorithm when rapid adaption times are desired arises because of the slower response time of the adaptive control loops to the weaker interfering sources. For an interfering source having power level P, the loop response time varies approximately as 1/P. Thus the dyanmic range of power levels to be nulled sets the dynamic range of adaption times required by the adaptive algorithm. On the other hand, in order to avoid the problem of "noisy loop" response, as discussed by Gabriel and Brennan, et al.,[2] the loops must be constrained from responding too rapidly. This condition is met by requiring

that the closed-loop bandwidth not exceed a small fraction of the nulling bandwidth BW, where we assume white noise interfering signals exist over the bandwidth BW. Thus the loops should respond no faster than approximately 5/BW seconds, and no longer than t_a, where t_a is the desired adaption time. Hence the dynamic range of power levels which the algorithm can handle is limited to approximately BW $\cdot$ $(t_a/5)$. Since the dynamic range of interfering sources may be as high as, say, 50 dB, this could require operation of the loops over a large nulling bandwidth when fast adaption times are desired. However, as the nulling bandwidth increases, the interference rejection capability inherent in the particular antenna configuration generally decreases, and tradeoffs must then be made.

The spread in adaption times vs interference power level is related to the spread in the eigenvalues of the interfering-source correlation matrix defined at the receive beam ports. By compressing this eigenvalue spread, we can increase the dynamic range sensitivity of the algorithm. Three techniques for accomplishing this, particularly applicable to multiple-beam antennas, will be discussed:

(a) Pre-weighting at the receive beam ports

(b) Incorporation of a hard limiter in each element feedback loop

(c) Increasing the number of beams over a fixed field of view.

For the present study, it is assumed that the interfering sources incident on the aperture (i.e., referred to 0 dB antenna gain) range from 0 to 55 dB above the system thermal noise level over the nulling bandwidth. It

is desired to "sense" and minimize those sources having power levels in a specified dynamic range below the maximum, in minimum adaption time. We assume that the residual desired-signal-to-interference ratio after spatial adaption, resulting from either the weaker interfering sources or the effects of bandwidth, can be further enhanced by some type of post-processing (e.g., spread spectrum techniques). Further, it is assumed that the desired signals received by the MBA are at a power level below that which the loops can "sense", and hence are minimized by the algorithm only as a consequence of their proximity to an interfering source.

The proposed communications system is designed to serve a multitude of users simultaneously, the positions of which are assumed unknown and randomly located. Since the number of users can be as large as 50 or so, the principal mode of operation of the MBA is assumed to be that of earth coverage; i.e., the desired radiation pattern of the antenna is designed for minimum gain deviation, but maximum gain, over the earth FOV. The special cases of known user positions (maximum signal mode) are handled by steering a maximum gain beam to the general vicinity of a known set of users. Adaption can occur in either mode of operation.

The analysis to follow begins with a brief discussion of some of the basic properties of the MBA configuration used in the study. Some of the properties of the conventional LMS power minimization algorithm as they apply to the MBA are then developed. Finally, the eigenvalue compression techniques are considered.

II. Antenna Modeling

Since the quality of the adapted radiation pattern is inherently related to the properties of the antenna used in conjunction with the adaptive algorithm, it is useful to digress and discuss the characteristics of the assumed antenna configuration. The MBA illuminates the earth with a fixed-position set of beams which are chosen to cover the desired FOV. The fundamental nulling limitations of such an antenna, and optimum beam positioning for nulling, have been discussed in Ref. 3. For earth-coverage illumination the beams are positioned hexagonally, and labeled as shown in Fig. 1a for seven beams and Fig. 1b for 19 beams. The extension to 37 and 61 beams follows straightforwardly. The seven beam system is of particular interest since it represents the smallest antenna diameter which can be used, and yet illuminate the FOV in the hexagonal manner shown. The corresponding seven antenna ports yield the minimum number of adaptive loops needed for adaptive control of the radiation pattern. As the number of beams increases, the aperture diameter increases, so that the smaller beamwidth obtained allows for full coverage over the FOV. It has been demonstrated[3] that beam positioning is a significant factor in obtaining good nulling resolution. For our antenna model, the beams are positioned in a hexagonal array defined by the angular positions

$$\theta_{n,m} = \sin^{-1}\left\{\left(\frac{\lambda}{\pi D}\right) \alpha \sqrt{u_n^{\,2} + v_{n,m}^{\,2}}\right\} \tag{1a}$$

$$\phi_{n,m} = \tan^{-1}\left(v_{n,m}/u_n\right) \tag{1b}$$

where

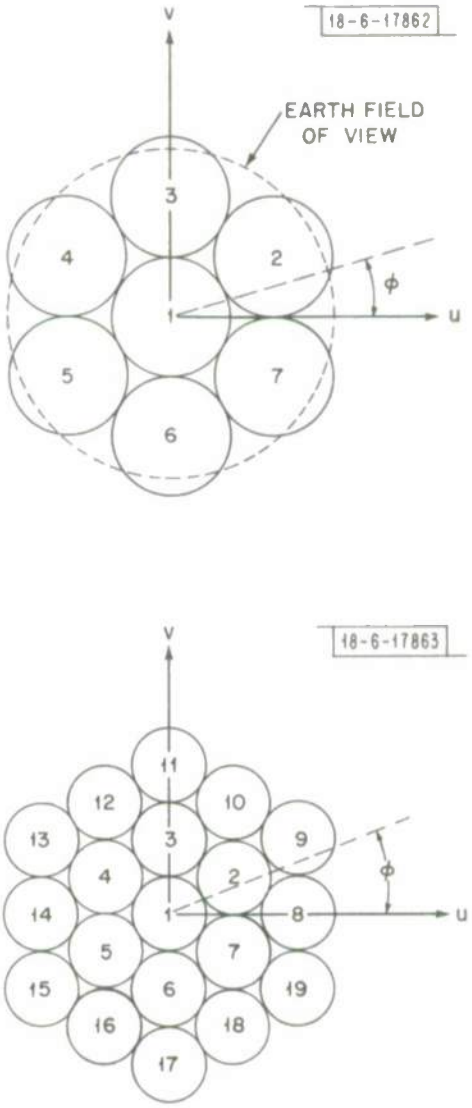

Fig. 1. 7- and 19-MBA beam positioning and labeling for earth-coverage FOV.

$$u_n = \alpha n\pi \tag{2a}$$

$$v_{n,m} = \alpha \frac{\pi}{\sqrt{3}} (2m-n) \tag{2b}$$

and α is the beam placement parameter determining the radial positioning of each beam. The integers n,m range either positive or negative so as to position the beams as desired for 7, 19, 37 or 61 positions. The inner ring of beams is positioned according to

$$\sin\theta_B = \frac{2}{\sqrt{3}} \alpha \left(\frac{\lambda}{D}\right) = \frac{2}{\sqrt{3}} \alpha \text{ (HPBW)} \tag{3}$$

where θ_B denotes the beam position and HPBW the half-power beamwidth. The latter form of Eq. (3) should be used for aperture illuminations other than uniform. For a lens or reflector system, physical realization of θ_B would be obtained by off-setting an array of feeds from the focal point of the lens or reflector, transverse to the focal axis. In this case

$$\theta_B = \delta \tan^{-1}(d/F) \tag{4}$$

where d is the feed separation, δ the beam deviation factor (see, for example, Ref. 4) and F the focal length. Using (4) in (3), and assuming $d << F$, we obtain

$$\alpha = \delta \frac{\sqrt{3}}{2} \left(\frac{d}{\lambda}\right) \cdot \frac{(\lambda/D)}{\text{HPBW}}/(F/D) \tag{5}$$

Equation (5) conveniently expresses α in terms of the feed spacing, in wavelengths, and the F/D ratio of the lens or reflector. For optimum nulling resolution, $\alpha \lesssim 1$.[3] However, depending on the desired aperture illumination,

the physical size of the feed element dictates a minimum allowable (d/λ). Furthermore, for a fixed D/λ, placement of the beams according to $\alpha = 1$ can lead to some loss in gain towards the edge of the FOV. Consequently, physical constraints other than nulling resolution often require a choice of $\alpha > 1$, particularly for a small number of beams. Once α is chosen according to Eq. (5), any adjacent beams are essentially equally spaced over the narrow earth FOV as viewed from synchronous altitude.

Table 1 below summarizes the particular choices of α and D/λ used in the following study. The value of D/λ used for a particular set of beams is only meant to be representative of a particular design, and was not optimized in any way. For seven beams, a value for a slightly greater than unity was chosen in order to improve the coverage area toward the edge of the FOV.

Table 1

D/λ and α vs Number of Beams

No. of Beams	D/λ	α
7	10.7	1.18
19	16.1	1.0
37	25.0	1.0
61	30.3	1.0

The beams used in the study are the maximum directivity, $J_1(x)/x$ beams described in Ref. 3, where $J_1(x)$ is the Bessel function of the first kind having argument x, and are positioned according to Eqs. (1). The beam positions do not change with frequency, which is indicative of a reflector or lens type MBA; hence, the frequency sensitivity of the antenna is somewhat more broadband when compared to an MBA using a frequency sensitive beam-forming network.

In Sections II and III, we consider in detail the operation of a seven-beam system, and defer the larger MBA types to the later sections.

III. Basic Properties of the Modified Applebaum-Howells Adaptive Control System

Consider the K-element adaptive control system illustrated in Fig. 2. Denote the signals received at the output of each feed-port as $E_1,\cdots,E_K$. Since the assumed set of beams characterizing the response to each feed element are functions of frequency, it is more useful for our purposes to interpret the received signals, E_k, in the frequency domain. The time variation of the control weights $w_1,\cdots,w_K$ are governed by a set of K first-order differential equations, which can be expressed in the form[1]

$$\underline{dw}/dt + \frac{1}{\tau}\{\underline{\underline{I}} + \mu_o \underline{\underline{R}}\} \cdot \underline{w} = \frac{1}{\tau}\underline{V}_a \tag{6}$$

The interpretation of the constants appearing in Eq. (6) has been discussed in some detail in Ref. 1. Briefly, τ is the open-loop time constant of the correlator, $\mu_o = k^2GN$, where k^2 is a mixer constant, G the open-loop gain and N is the thermal noise level over the bandwidth BW, assumed identical in each channel. Although N is a function of the filter bandwidth BW, the loop gain G can be set as desired for a particular bandwidth under consideration. Hence μ_o can be interpreted as a constant parameter. $\underline{\underline{R}}$ is the cross-correlation matrix for the normalized voltages at each receive port,

$$\underline{\underline{R}} = \overline{E_k E_q}, \tag{7}$$

where the superbar denotes the average over the frequency band BW,

$$(\cdot) \equiv \frac{1}{BW}\int_{\omega_o - \frac{BW}{2}}^{\omega_o + \frac{BW}{2}} (\cdot)\, d\omega \tag{8}$$

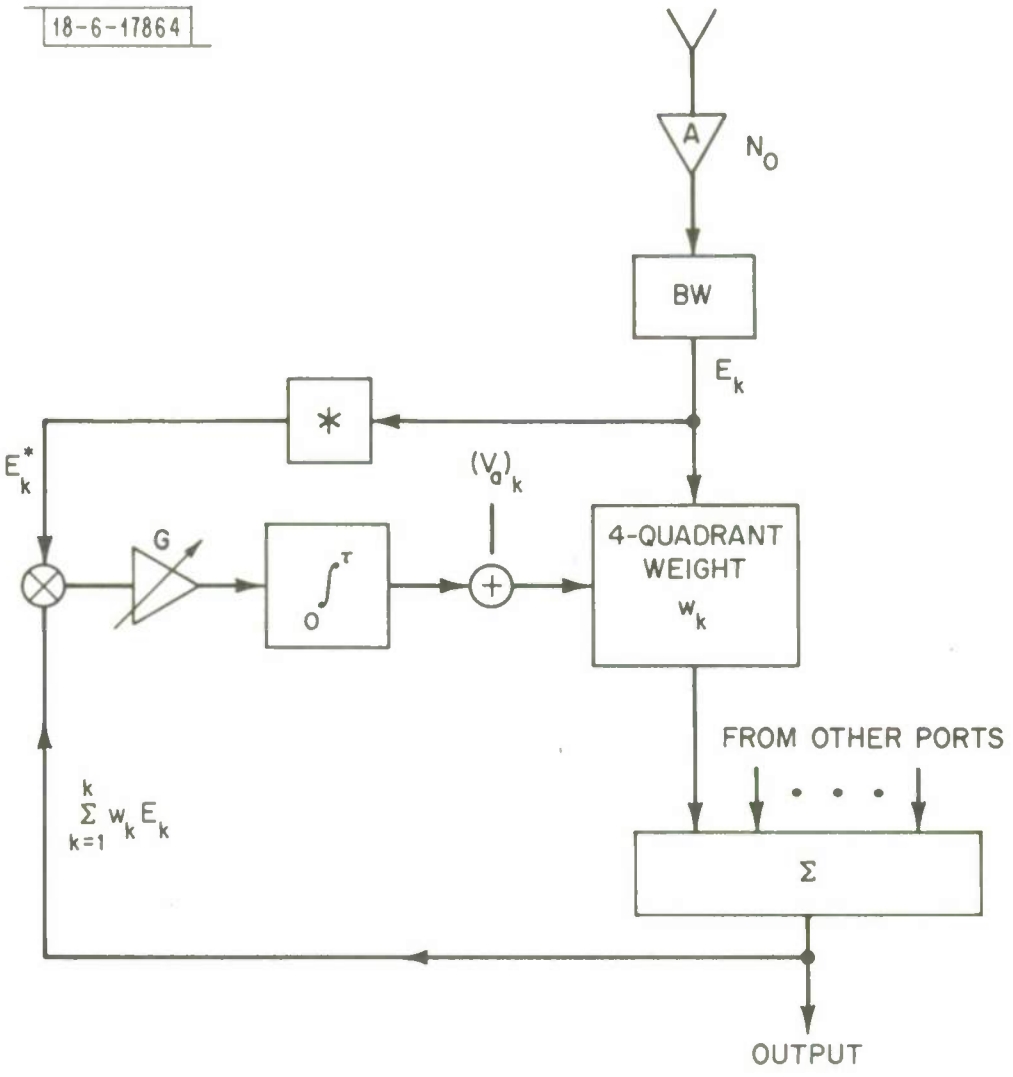

Fig. 2. Control mechanism for the kth complex weights.

and ω_o denotes the center-band frequency. Assuming a reactively matched receive network, we show in Appendix B that $\underline{\underline{R}}$ can be expressed in the form (for the case of J narrowband, incoherent interference sources)

$$\underline{\underline{R}} = \sum_{j=1}^{J} R_j \left(\frac{4\pi A}{\lambda^2}\right) 4\, \underline{\underline{D}}^{-1} \cdot \overline{\underline{c}_j \underline{c}_j^{\dagger}} \cdot \underline{\underline{D}}^{-1} + \underline{\underline{I}} + 4\, e_o\, \underline{\underline{D}}^{-1} \cdot \underline{\underline{R}}_N \cdot \underline{\underline{D}}^{-1} \qquad (9)$$

where R_j denotes the ratio of the interference power density (in watts/m^2) for the jth source incident on the aperture (i.e., referred to 0 dB antenna gain) to internal thermal noise density N_o; $(4\pi A/\lambda^2)$ is the maximum antenna gain for an aperture of area A; $\underline{\underline{R}}_N$ is the real part of the impedance matrix $\underline{\underline{Z}}$ characterizing the antenna ports upon transmission, normalized to the characteristic impedance R_o of the feed transmission lines; i.e.,

$$\underline{\underline{R}}_N = \mathrm{Re}(\underline{\underline{Z}})/R_o. \qquad (10)$$

$\underline{\underline{D}}$ is the matrix $\underline{\underline{I}} + \underline{\underline{R}}_N$ and $\underline{c}_j$ is a column vector of the beam patterns for each isolated port, evaluated at the interference-source coordinates (θ_j, ϕ_j), and normalized to 0 dB at the peak of each beam. e_o is the ratio of external to internal noise temperature, T_e/T_i. Assuming 1000°K preamps, and $T_e \approx 300$°K, then $e_o = 0.3$. The constant R_j can be written in the form

$$R_j = \frac{P_j G_j (\lambda/4\pi R)^2}{N_o (\mathrm{SBW})} \qquad (11)$$

where $P_j G_j$ is the effective radiated power (ERP) of the jth interfering source assumed spread uniformly over a fixed bandwidth, SBW, and $(\lambda/4\pi R)^2$ is the path loss to the satellite. It is assumed throughout that SBW > BW.

In order to evaluate the beam steering weights $\underline{V}_a$, it is convenient to separate the matrix $\underline{\underline{R}}$ into an interference matrix $\underline{\underline{M}}_I$ and noise matrix $\underline{\underline{M}}_N$. We define

$$\underline{\underline{R}} \equiv \underline{\underline{M}}_I + \underline{\underline{M}}_N \tag{12}$$

where

$$\underline{\underline{M}}_N = \underline{\underline{I}} + 4\, e_o\, \underline{\underline{D}}^{-1} \cdot \underline{\underline{R}}_N \cdot \underline{\underline{D}}^{-1} \tag{13}$$

Then $\underline{\underline{M}}_I = 0$ in the absence of interfering sources. In this case Eq. (6) reduces to the quiescent condition:

$$\frac{1}{\beta_o}\, \underline{V}_a = [\underline{\underline{I}} + \mu_o\, \underline{\underline{M}}_N] \cdot \underline{w}_o \tag{14}$$

where $\underline{w}_o$ is a column vector of the desired weights; i.e., that set of weights which determine the desired radiation pattern in the absence of interfering sources. Thus the beam steering voltages $\underline{V}_a$ offer a direct means of controlling the weights in the absence of interfering sources. By properly choosing the $\underline{V}_a$, quiescent weights $\underline{w}_o$ can be determined which result in the desired radiation pattern when no interfering sources are present.

The time evolution of the weights from their initial value $\underline{w}_o$ to the steady state value $\underline{w}_{ss}$ can most conveniently be expressed in terms of the eigenvalues and eigenvectors of $\underline{\underline{R}}$. We define these according to

$$\underline{\underline{R}} \cdot \underline{e}_k = s_k\, \underline{e}_k \tag{15}$$

Solutions for $\underline{w}(t)$ then can be written in the form

$$\underline{w}(t) = \sum_{k=1}^{K} \underline{e}_k (\underline{e}_k^{\dagger} \cdot \underline{w}_o)\ (\tau_k/\tau)\ [1 + \mu_o\, s_k\, e^{-t/\tau_k}]$$

$$+ \mu_o \sum_{k=1}^{K} (\tau_k/\tau)\ \underline{e}_k (\underline{e}_k^{\dagger} \cdot \underline{\underline{M}}_N \cdot \underline{w}_o)\ [1 - e^{-t/\tau_k}] \qquad (16)$$

where the K time constants τ_k are defined by

$$\tau_k = \frac{\tau}{1 + \mu_o\ (1 + s_k)} \qquad (17)$$

and the notation "$\dagger$" denotes "complex-conjugate, transpose". The time constants τ_k essentially determine the adaption time. We note that all $\tau_k \leq \tau$, so that the open-loop integration time sets an upper bound on the convergence rate. Thus the K time constants can be ordered according to $\tau_{MIN}, \cdots, \tau_{MAX} \approx \tau$. The eigenvalues s_k determining the τ_k are a strong function of nulling bandwidth BW, interference power level, and interference scenario. We note however that although the spread in the eigenvalues s_k may be quite large, the corresponding spread in the time constants τ_k can be made considerably smaller by reducing the loop gain μ_o. Otherwise said, if μ_o is reduced sufficiently, the loops do not sense the weaker interfering sources. Hence by properly choosing μ_o, a tradeoff can be made between speed of adaption and the dynamic range of interfering sources to be minimized. For this study, assuming interfering sources incident on the aperture ranging from 0-55 dB above thermal noise, the loop gain μ_o is set so that only the larger interfering sources

are minimized (e.g., those lying between 25 and 55 dB above thermal noise) using radiation pattern shaping, but in a rapid time frame, while the remaining weaker sources are reduced by post-processing after spatial adaption has taken place. The consequences of such a choice for μ_o are discussed in this and the following section, and eigenvalue compression techniques for eliminating some of the problem areas which arise are considered in Section V.

After adaption has taken place, the steady state solution for the weights can be determined from Eq. (6) by setting $d\underline{w}/dt = 0$. We obtain

$$\underline{w}_{ss} = [I + \mu_o \underline{\underline{M}}_J + \mu_o \underline{\underline{M}}_N]^{-1} \cdot \underline{V}_a \tag{18}$$

Since $\mu_o << 1$ for the reasons discussed above, Eq. (18) reduces to

$$\underline{w}_{ss} \approx [\underline{\underline{I}} + \mu_o \underline{\underline{M}}_J]^{-1} \cdot \underline{w}_o \tag{19}$$

In Appendix A we show that this steady state solution is equivalent to minimizing the total output power of the array, relative to the effective noise level, N/μ_o, such that the resulting steady state weights give the best mean square approximation to the desired weight $\underline{w}_o$. In the presence of a single user, and with $\underline{w}_o$ chosen to point a maximum directivity beam towards that user, this is equivalent to maximizing the received signal/interference power ratio as shown by Gabriel, where the desired weights are chosen to steer a maximum directivity beam to the single user. For more than a single user, the steady state solution, Eq. (19), is equivalent to minimizing the total output power of the array, simultaneously resulting in the best RMS approximation to the desired radiation pattern. This will be demonstrated by

simulations later in this section, and is further discussed in Appendix A.

Since the interference power and interference source location cannot be controlled, we essentially have three parameters over which to optimize the loop performance: τ, μ_o (or loop gain G) and BW. However these cannot be varied independently, and we now enumerate the two constraints which ultimately determine their values.

(A) Minimum Loop Convergence Time

As developed by Brennan, et al.[2] the actual evolution of the weights $\underline{w}(t)$ in a wideband interference environment is characterized by a sample function of a random noise process. Thus the time evolution of $\underline{w}(t)$ is not characterized by the smooth variation of Eq. (16), but rather a noisy variation with Eq. (16) specifying the expected value of the weights. They have shown that the expected value of the normalized output power is given by

$$\langle P_o \rangle = \underline{w}^{\dagger} \cdot \underline{\underline{R}} \cdot \underline{w} \left\{1 + \left(\frac{\mu_o}{2\tau \cdot BW}\right) \sum_{k=1}^{K} s_k\right\} \tag{20}$$

For the adaptive circuitry to realize its full nulling capability, the second term in (20) must be kept small relative to unity. Assuming a single large interfering source dominates the scenario, we approximate $\sum_{k=1}^{K} s_k \approx s_{MAX}$. The second term can then be approximated as

$$\frac{\mu_o}{2\tau \cdot BW} \cdot s_{MAX}$$

This term can be expressed in terms of the minimum time constant τ_{MIN}. Using (17), assuming $\mu_o s_{MAX} >> 1$, we have

$$\tau_{MIN} \approx \frac{\tau}{\mu_o \, s_{MAX}} \tag{21}$$

Thus the second term in (20) is essentially $\frac{1}{2\tau_{MIN} \cdot BW}$, and we require $\frac{1}{2\tau_{MIN} \cdot BW} << 1$. A reasonable value to use is, say, 0.1; we obtain $\tau_{MIN} \cdot BW = 5$. This leads to the first relationship between the three parameters τ, BW and μ_o:

$$(BW) \cdot \tau = 5 \, \mu_o \, s_{MAX} \tag{22}$$

(B) Dynamic Range

The dynamic range of the interfering sources essentially dominates the eigenvalue spread $\{s_k\}$ and hence the spread in time constants. Using (21), we estimate the dynamic range of power levels, DR, which the loops "sense" according to

$$DR \approx \frac{\tau_{MAX}}{\tau_{MIN}} \approx \frac{\tau}{\tau_{MIN}} = \mu_o \, s_{MAX} \tag{23}$$

Equation (23) conveniently expresses the dynamic range of the loop sensitivity in terms of the effective loop gain, μ_o, and maximum interference power level, s_{MAX}, which is proportional to $(I/N)_{MAX}$.

Equations (22) and (23) can be combined to illustrate the basic tradeoffs limiting the operation of the Applebaum-Howell control loop. Expressing (22) in terms of dynamic range, we have

$$(BW) \cdot \tau = 5 \, (DR) \tag{24}$$

Thus to obtain a large dynamic range one either has to increase the bandwidth

or increase the adaption time τ. (Note, we have implicitly chosen τ = desired adaption time so that we are assured steady state will be reached in the desired time. The alternate possibility of increasing τ and μ_o significantly, but "freezing" the weights at time $t_f \equiv$ desired adaption time, even though complete adaption has not taken place is also possible. In this case Eq. (21) implies that τ in Eq. (24) should be replaced by t_f.) Since the maximum allowable adaption time is essentially fixed at some prescribed value, the large dynamic range required must be obtained by increasing the nulling bandwidth BW. As we shall see later via simulation, as a consequence of reducing the loop gain μ_o, increasing the bandwidth leads to a larger residual output power after adaption, so that increasing the bandwidth does not necessarily result in achieving the desired dynamic range.

Before proceeding to some specific examples, it is instructive to develop a simple "rule of thumb" for the dyanmic range required to adequately handle a "worse-case" interference scenario. Generally if one desires to minimize, by spatial adaption, an interfering source power spread of say, 30 dB, one is tempted to conclude that only a 30 dB dynamic range is required. However since the residual interference powers after adaption add linearly, a larger dynamic range is required when more than one interference source is present. Say for example, that we design for a 30 dB dynamic range and three interfering sources--R_1 = 55 dB and $R_2 = R_3$ = 25 dB. The larger interfering source is reduced to a level either equal to or below the effective noise level, N/μ_o, depending on the bandwidth, whereas the smaller interfering sources are only slightly unaffected (assuming they are separated more than a beamwidth from

the large jammer). Since the powers from the two weaker interfering sources add linearly after adaption, the resulting interference level at the output after adaption is now at least 3 dB above the desired power reduction. An extension of this example leads to a simple criteria for the required dynamic range (RDR):

$$(\text{RDR}) = (\#\ \text{large sources}) + (R_j)_{\text{MAX}} + (\#\ \text{smaller sources}) - (R_j)_{\text{MIN}} \tag{25}$$

where all values are in dB. For six sources, assuming one large interfering source and five smaller sources at a level 30 dB below the larger source, at least 37 dB of dynamic range is require to adequately handle the worst-case scenario. For three large interfering sources and three smaller sources, a 39 dB dynamic range is required.

Consider now some specific examples to illustrate the basic behavior of the adaptive loops upon adaption. Assume we desire the MBA to adapt in 1.33 msec, and adapt to a six-source interference scenario having a 34 dB dynamic range in power level. Adaption in the desired time frame will be assured if we choose τ = 1.33 msec. Assuming a 10 MHz nulling bandwidth, Eq. (24) predicts a usable dynamic range of 34 dB. Although this is slightly less than the desired 37-39 dB dynamic range obtained using (25), it is pushing the limit of what can be obtained using conventional LMS loops adapting in 1.33 msec. If we further assume a single 55 dB interfering source dominates the scenario, then $s_{\text{MAX}} \approx 85$ dB (i.e., approximately 30 dB maximum antenna gain at any beam port using $D/\lambda \approx 10.07$). Applying Eq. (23)

gives μ_o = -51 dB. For example purposes, we assume the six interfering-source scenario given in Table 2 below

Table 2

Source	R_j (dB)	Location (θ_j, ϕ_j)
I_1	55	(7.33°, 30°)
I_2	25	(6° ,180°)
I_3	21	(7° ,270°)
I_4	21	(7.33°,120°)
I_5	21	(.01° , 0°)
I_6	21	(8° , 70°)

This represents somewhat of a "worse-case" scenario in that the wide spread in power levels takes advantage of the limited dynamic range available to the algorithm. Furthermore, source locations spread out uniformly, together with the 10 MHz nulling bandwidth, force the MBA to use all of its seven degrees of freedom. The desired pattern is chosen to be the earth-coverage pattern illustrated in Fig. 3. The contour levels indicate directive gain over the earth field of view as viewed from the satellite, accounting for the curvature of the earth. Thus the radial dimension ρ measured from the center of the FOV to a particular position on the earth is not linear with pattern angle as measured from the satellite, but varies according to

$$\tan\theta = \frac{\rho}{(R_e + h) - \sqrt{R_e^2 - \rho^2}} \tag{26}$$

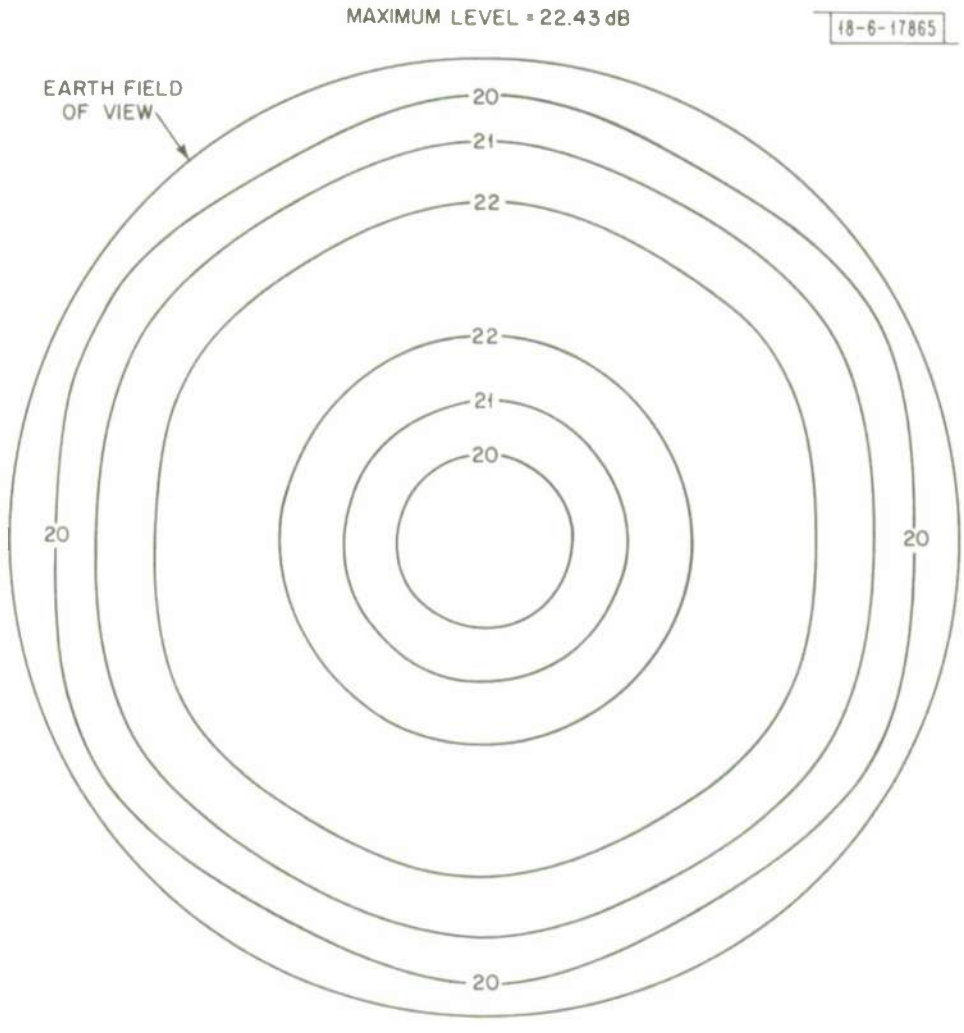

Fig. 3. Earth-coverage radiation pattern for seven beams, $D/\lambda = 10.07$, $\alpha = 1.18$.

where θ = pattern angle measured relative to the satellite axis, R_e = radius of earth and h = height of the satellite above the surface of the earth. The maximum directive gain available from the 10.07λ aperture is 30.5 dB. The contours in Fig. 3 are to be compared to an ideal earth-coverage gain of 23.2 dB.

Consider first the case where I_1 and I_2 are present. In Fig. 4, the time history of (I/N) at the output of the sum channel is illustrated for each source. As expected, the loops adapt in the specified time, 1.33 msec. We note the rapid adaption to the large interfering source and the relatively slow adaption of the weak source, as expected. Note also the <u>level</u> of adaption. Since the weak source was only approximately 4 dB above the effective noise before adaption, the corresponding spatial A/J is not very large. Otherwise said, I_2 appears to the loops as a source of strength $\mu_o(I_2/N)$, and is minimized relative to the effective noise level N/μ_o. This is illustrated in Fig. 5, in which we illustrate a directive gain contour plot of the adapted pattern at t = 1.33 msec. The adapted directivity in the direction of I_1 at the center-band frequency is $D(\theta_1,\phi_1)$ = -48 dB whereas, for I_2, $D(\theta_2,\phi_2)$ = 15.9 dB. Define I_t to denote the total interference power ΣI_j+N. The ratio of (I_t/N) before adaption to (I_t/N) after adaption is 34.3 dB--essentially equal to the dynamic range of the system. We note also that the weaker source essentially sets the level of the interference rejection--i.e., once a large source is present, many weaker sources then offer the greatest limitation to the system. The adapted level of I_1 is essentially determined by the percentage bandwidth (approximately 3% for the assumed

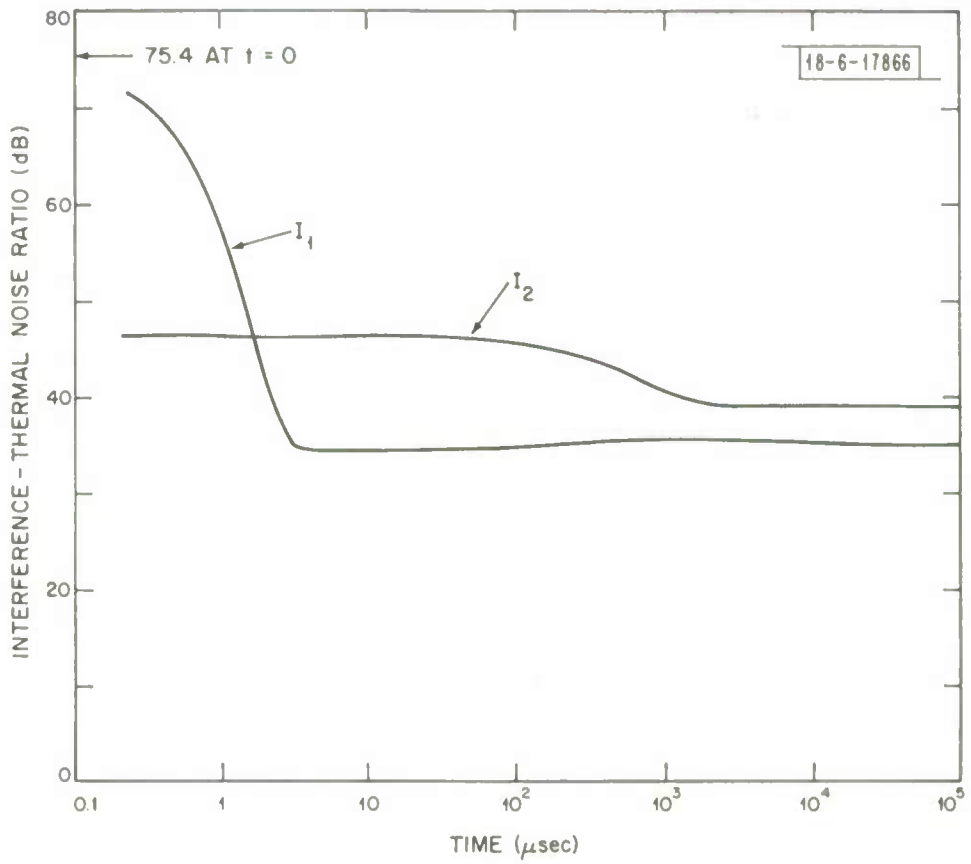

Fig. 4. Interference--Thermal noise ratio vs time for two-interfering sources I_1 and I_2 in Table 2. D/λ = 10.07 and FBW = .0286.

frequency). Decreasing the bandwidth would lower the adapted level. Conversely, significantly increasing the bandwidth would increase the adapted level, resulting in the larger source dominating the total interference output power. We also observe in Fig. 5 the earth-coverage pattern constraint is adhered to quite nicely over the field of view away from the large interfering source.

Figure 6 illustrates the time evolution, $w_k(t)/w_k(0)$, of each of the seven weights. Note in particular weight w_2, which essentially turns off beam 2 where the large source is located. Weights w_4 and w_5 (I_2 lies between beams 4 and 5) appropriately change after a much longer time. The four remaining weights are only slightly affected. Thus, the MBA serves to "decouple" the adaptive loops from each other, as contrasted to the phased array having an adaptive loop at each element, for which all weights would contribute significantly to the adapted pattern. Hence for a large number of beams, the problem of fabricating a large number of identical loops becomes less significant with the MBA, and maintaining error tolerances between loops should not be as critical as with an adaptive phased array. Also observe that the beam steering constraint acts as a first order AGC on the weights, i.e., adaption occurs so that $|\underline{w}-\underline{w}_o|^2$ is minimum. To illustrate this note that the loss in gain, relative to the weights at t = 0, due to weight variation is essentially determined by

$$\Delta G = \sum_{k=1}^{K} |w_k|^2 / \sum_{k=1}^{K} |w_k(t=0)|^2 \qquad (27)$$

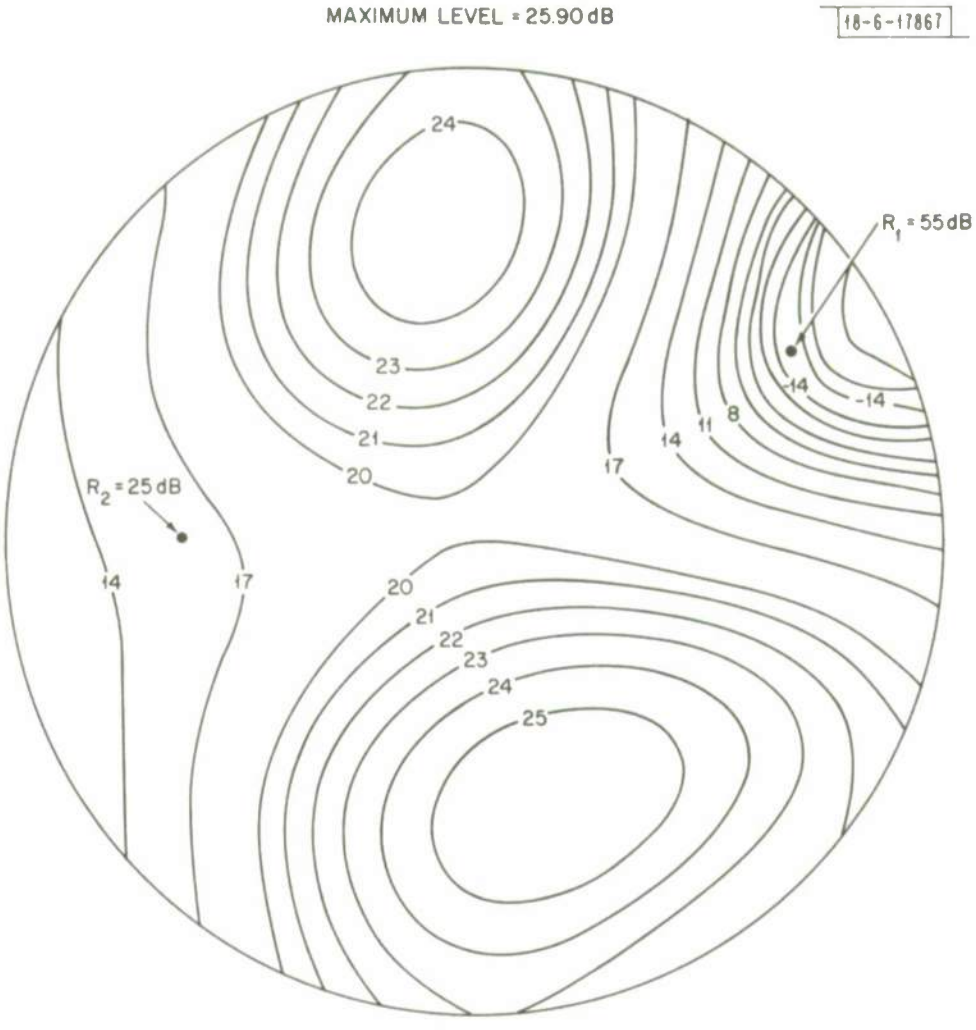

Fig. 5. Adapted radiation pattern for the two-interference source scenario of Table 2. D/λ = 10.07 and FBW = .0286.

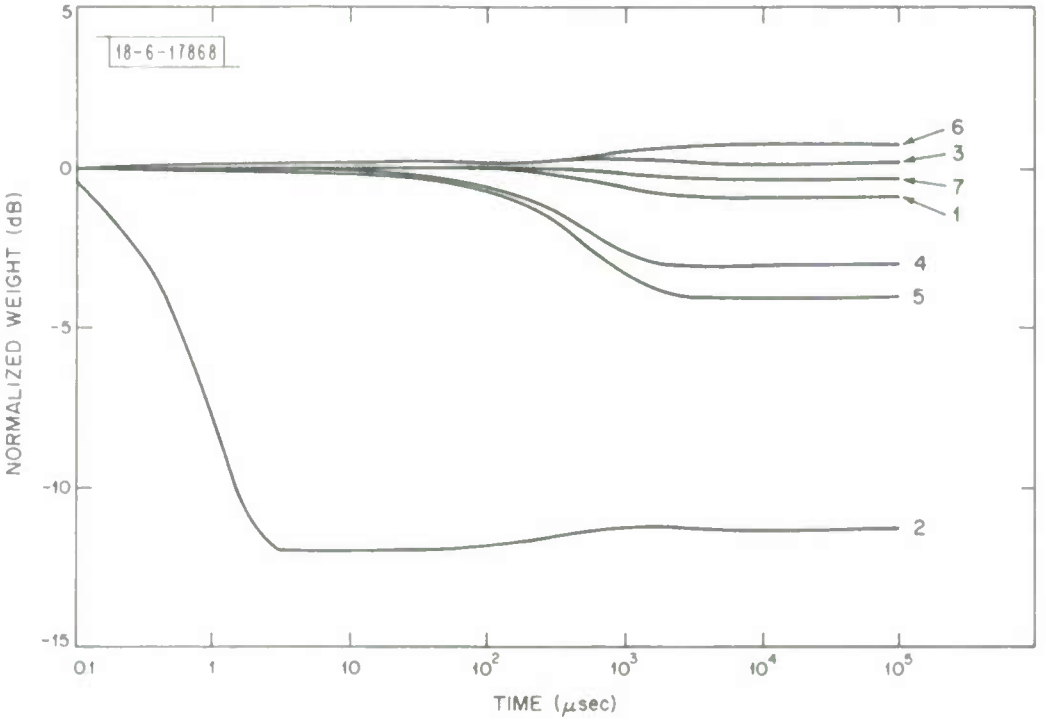

Fig. 6. Time adaption of weights for the two-interference source scenario of Table 2. D/λ = 10.07 and FBW - .0286.

ΔG is plotted as a function of time in Fig. 7. Observe only 2 dB loss in gain is encountered after adaption.

As an extreme case, consider now the presence of all six interfering sources in Table 2. We anticipate this as a worse case for the 34 dB dynamic range considered since the loops will respond only slightly to the weaker sources, but their powers add linearly after adaption. Thus the interference rejection should degrade by approximately 6 dB when compared to the two-source case. Figure 8 illustrates I/N for each of the six interfering-sources. As expected the weaker sources are only slightly affected, and the ratio of total interference/thermal noise ratio before adaption to that after adaption has decreased to 27.3 dB, seven dB lower than the two-source case. The adapted pattern at t = 1.33 msec is illustrated in Fig. 9. Note the deep null on I_1, whereas only relative minima are formed on the weaker sources. The change in gain due to the weight variation, ΔG, has increased to -4.9 dB.

Before proceeding to the next section, it is of interest to examine the behavior of the adapted weights for zero bandwidth. In this case, the criterion defined by Eq. (22) is violated, but since the output of the correlator is no longer random (i.e., as BW $\rightarrow$ 0 the antenna port outputs become perfectly correlated), there is no need to insure against random noise driving the weights. The interference/thermal noise ratio for the two-source scenario considered previously is plotted in Fig. 10 for this case. Note in particular the much larger reduction in (I_1/N) for the larger jammer when compared to Fig. 4. For c.w. sources, the level of reduction of (I_1/N) essentially lies as far below (in dB) the effective noise level as the inter-

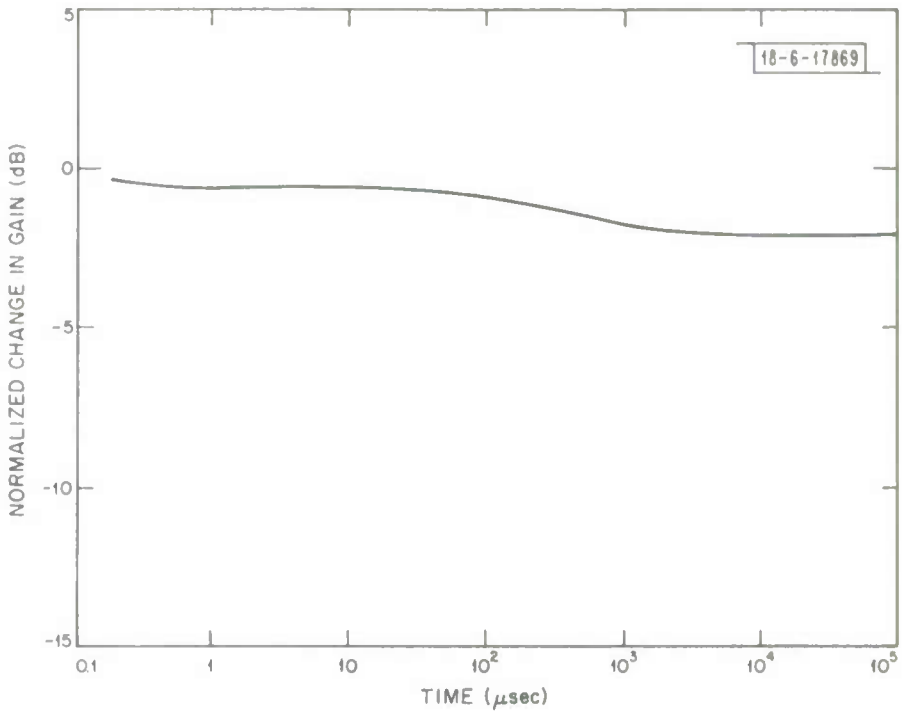

Fig. 7. Loss in gain due to weight variation for two-source scenario of Table 2. $D/\lambda = 10.07$ and FBW = .0286.

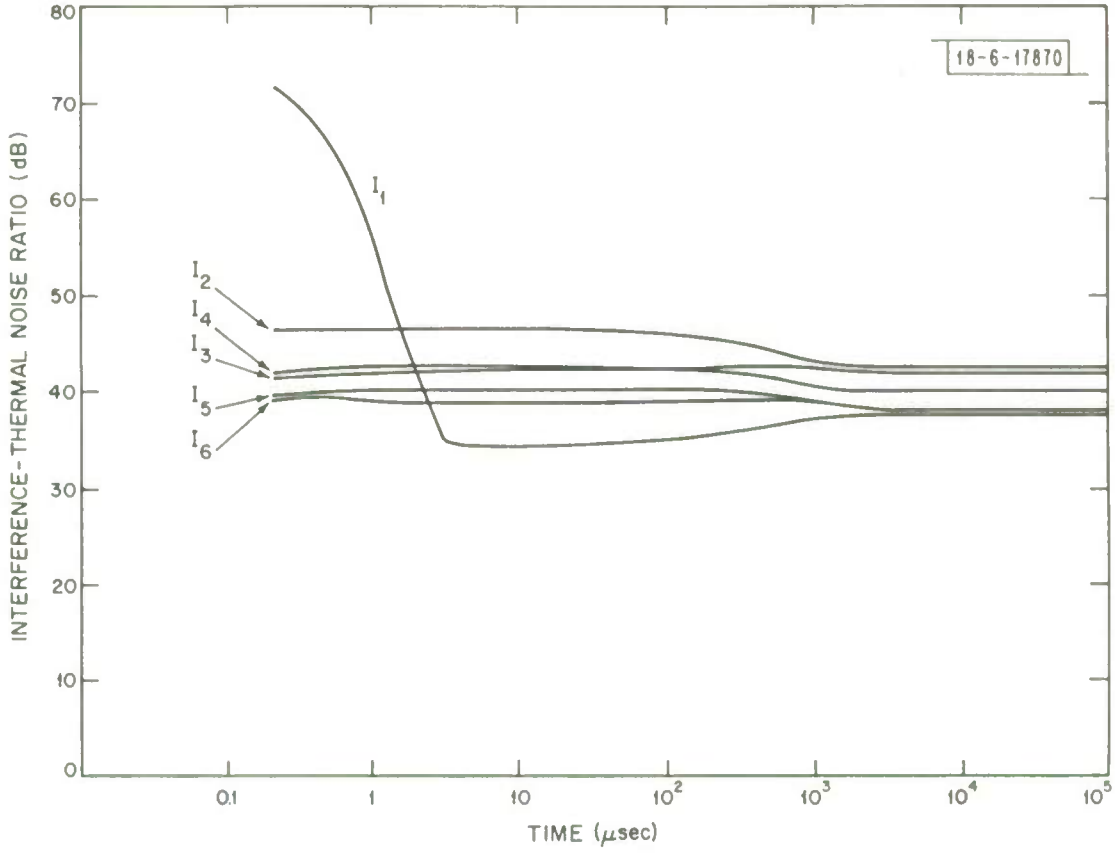

Fig. 8. Interference--Thermal noise ratio vs time for the six-source scenario of Table 2. D/λ = 10.07 and FBW = .0286.

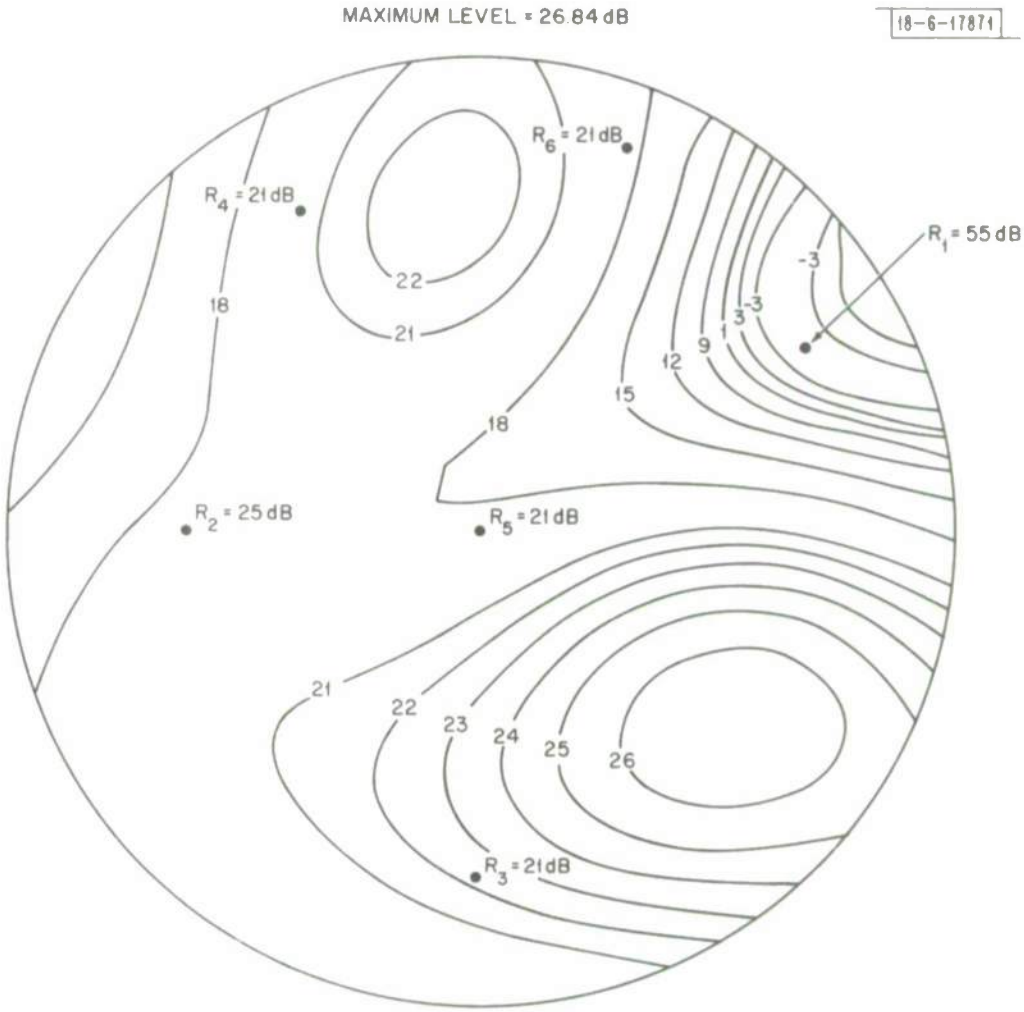

Fig. 9. Adapted radiation pattern for the six-source interference scenario of Table 2. D/λ = 10.07 and FBW = .0286.

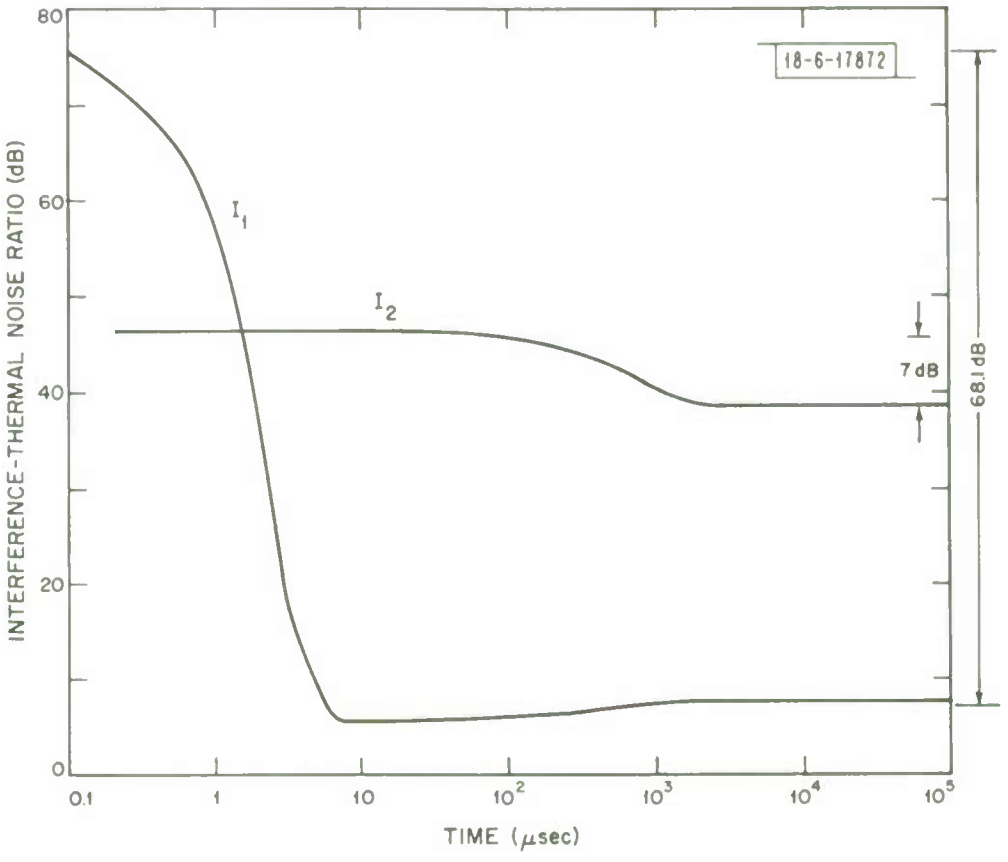

Fig. 10. Interference--Thermal noise ratio vs time for two-sources I_1 and I_2 of Table 2. D/λ = 10.07 and FBW = 0.

ference was above (in dB) the effective noise before adaption. We define the parameter $\Delta(I/N)$, measured in dB, as a measure of the interference suppression realized by the algorithm:

$$\Delta(I/N) \equiv [(I/N)_b]_{dB} - [(I/N)_a]_{dB} \tag{28}$$

where the subscript "b" denotes before adaption and "a" after adaption. This is indicated in Fig. 10 for each source. Note the change $\Delta(I/N)$ for the largest source corresponds to twice the dynamic range when expressed in dB. For interference sources in close proximity to each other, the "rule of thumb" only holds for the larger source, as the smaller source will be reduced an added amount due to the pattern change near the null formed on the large source.

Finally consider the special case of large, c.w. interfering sources only--i.e., all sources are assumed to be, say, at least 20 dB above the effective noise level. In this case, the Applebaum-Howell algorithm adapts so as to place a "null" on each source, simultaneously prescribing the best rms fit to the desired radiation pattern using the available degrees of freedom. Consider a particular example. Figure 11 illustrates the directive gain contour over the earth FOV obtained using the adapted weights for two large sources placed at ($\theta_1 = 4°$, $\phi_1 = 30°$) and ($\theta_2 = 6°$, $\phi_2 = 180°$). Figure 12 illustrates the directive gain contour over the earth FOV computed using pattern synthesis of an earth-coverage radiation pattern with two constrained nulls at the assumed positions.[3] The similarities in the two results are readily apparent. Similar results were obtained using the maximum signal mode of operation. The reasons for the similarity are further discussed in Appendix B.

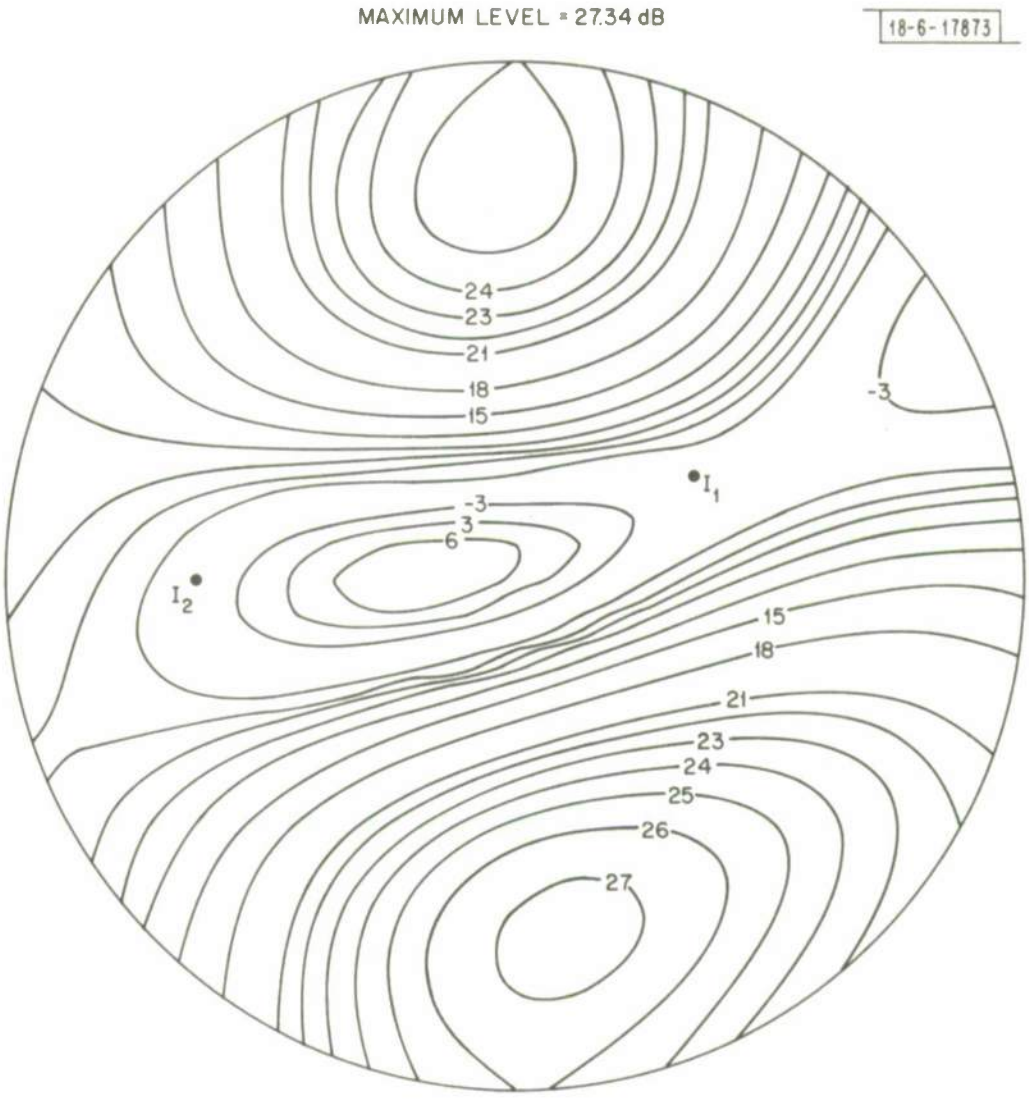

Fig. 11. Adapted radiation pattern for two large sources I_1 and I_2 using conventional LMS algorithm. $D/\lambda = 10.07$.

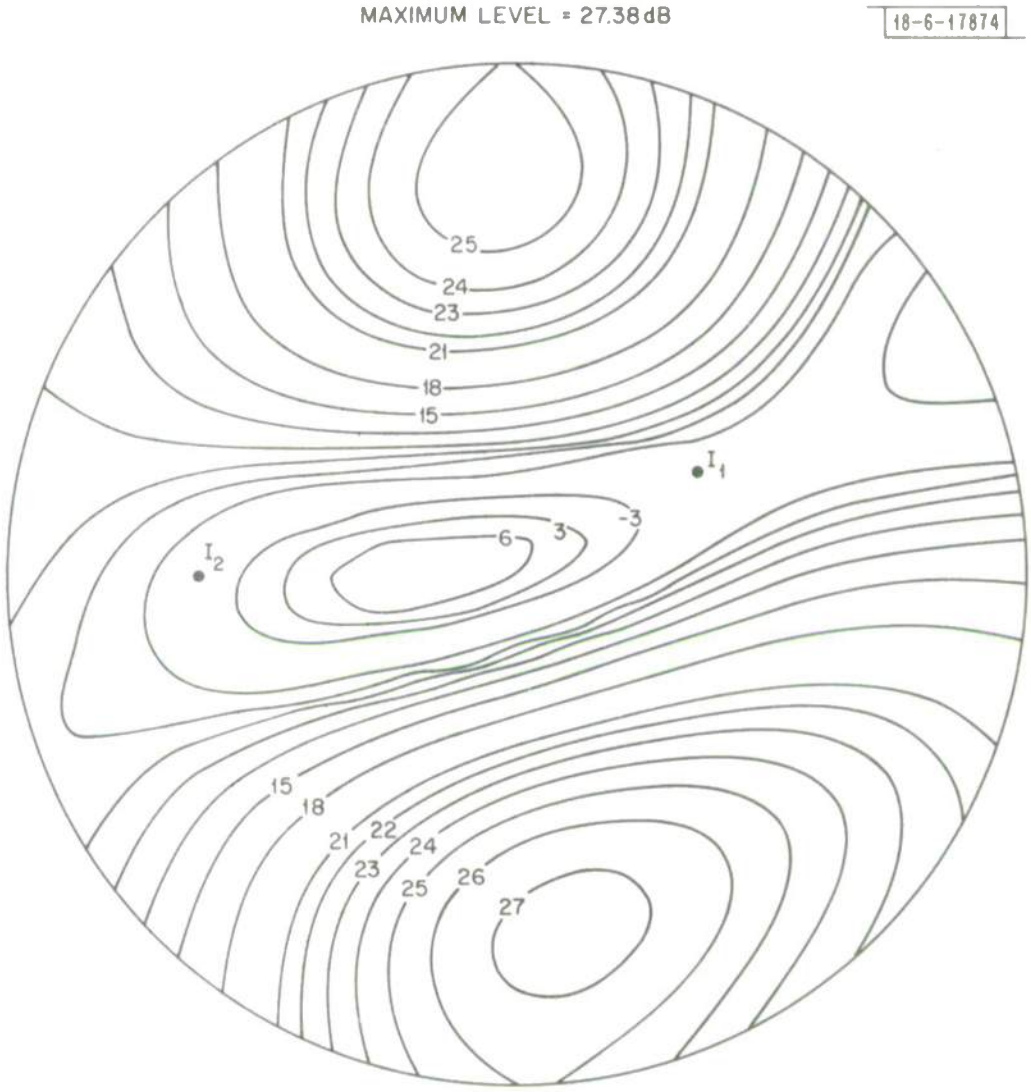

Fig. 12. Radiation pattern using pattern synthesis for nulls on I_1 and I_2. $D/\lambda = 10.07$.

IV. Bandwidth Effects and Signal-Interference Proximity

Since it is desirable to operate the adaptive loops over as wide a bandwidth as possible, in order to increase the dynamic range, for a fixed adaption time, it is useful to examine in detail the effects of increasing bandwidth. The bandwidth behavior of the adapted pattern is inherently a function of the effective loop gain μ_o. The effect of increasing bandwidth in a fixed interference scenario is manifested by way of the eigenvalues $\{s_k\}$ of the correlation matrix $\underline{\underline{R}}$ defined in Eq. (15). Define $s_o \simeq 1.3$ to be the normalized thermal noise level (internal plus external) of the system over BW. For bandwidths approaching zero and J interfering sources, only J of the $\{s_k\}$ are greater than s_o. As the bandwidth increases, the remaining eigenvalues gradually begin to increase above s_o. However, the ability of the loops to react to this increase in output power level occurs by way of the time constants $\{\tau_k\}$, which are a function of the product $\mu_o s_k$. Clearly, from Eq. (17), the τ_k can only change with variations in the s_k so long as $\mu_o s_k \gtrsim 1$. For a small increase in bandwidth, additional power occurs at the array output and, since $\mu_o s_{J+1} \ll 1$, is not sensed by the control loops. Thus the interference suppression capability of the array deteriorates with increasing bandwidth until a critical threshold is reached when $\mu_o s_{J+1} \simeq 1$. To demonstrate this, Fig. 13 illustrates the total interference suppression, $\Delta(I_t/N)$, vs FBW for three single-source scenarios having $R_1 = 55$ dB. The particular source locations were taken to be at the peak of beam 2, between beams 1, 2 and 7, and between beams 2 and 7 at the edge of the FOV, as illustrated in the figure. An earth-coverage constraint was used, but the behavior differs little from the maximum signal

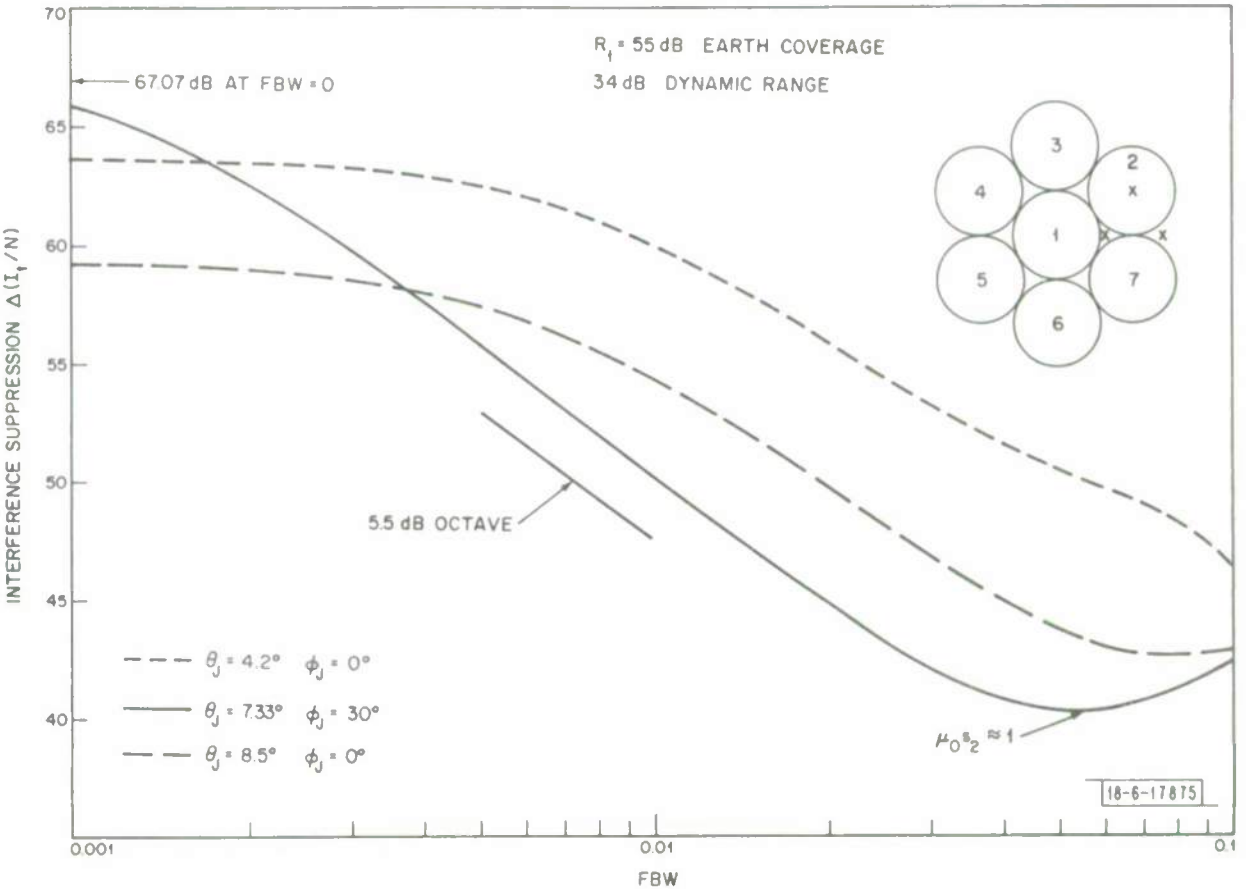

Fig. 13. Interference suppression, $\Delta(I_t/N)$, vs FBW for three single-interference scenarios as indicated.

constraint. The dynamic range is 34 dB, using the loop parameters selected in Section III. Observe that in all three cases, as FBW increases, the interference suppression capability initially decreases with increasing bandwidth, as discussed above. We have indicated on the curve the transition region $\mu_o s_2 \simeq 1$, at which point the array begins to "sense" the increase in interference power as the bandwidth widens. The interference suppression then begins to increase. The changes in the eigenvalue spectrum as a function of increasing bandwidth for the three interference scenarios considered is illustrated in Fig. 14. A 51 dB effective noise level is used to achieve a dynamic range of 34 dB. Notice that the region where $\mu_o s_2$ has increased to unity occurs for all scenarios between FBW = .05 - .08. Before this transition region is reached, the radiation pattern remains essentially unchanged from the FBW = 0 value. The increase in output interference power for each case as FBW increases from 0 is thus due to the bandwidth spread about the sharp null developed on the interfering source for 0 bandwidth. The output interference power increases approximately as the square of the bandwidth (actually 5.5 dB/octave). To further illustrate these concepts, we compare in Fig. 15 the adapted pattern, evaluated at the interfering source location when the source is at a beam maximum, vs frequency for FBW = 0 and FBW = .15, the latter case corresponding to $\mu_o s_2 >> 1$ so that the array has adapted to compensate for the wideband interfering source. Note that a higher level, but wider band, null has been formed on the interfering source.

It is interesting to compare the results of Fig. 13 for μ_o = -51 dB to the case when the effective loop gain is set to unity. Figure 16 illustrates the interference suppression, $\Delta(I_t/N)$, vs FBW for this case, using a 34 dB

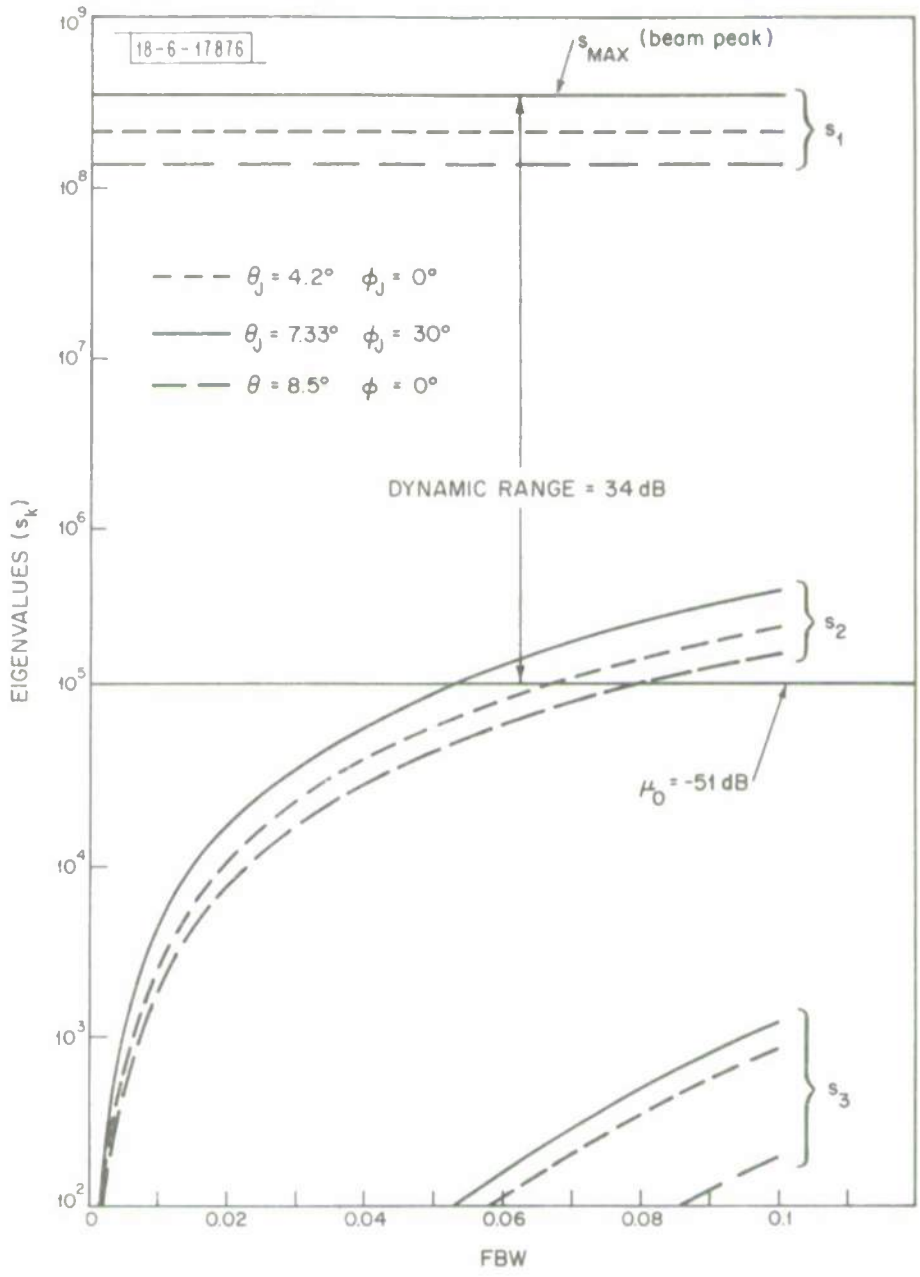

Fig. 14. Eigenvalue spectrum vs FBW for the three interference-source scenarios indicated in Fig. 13.

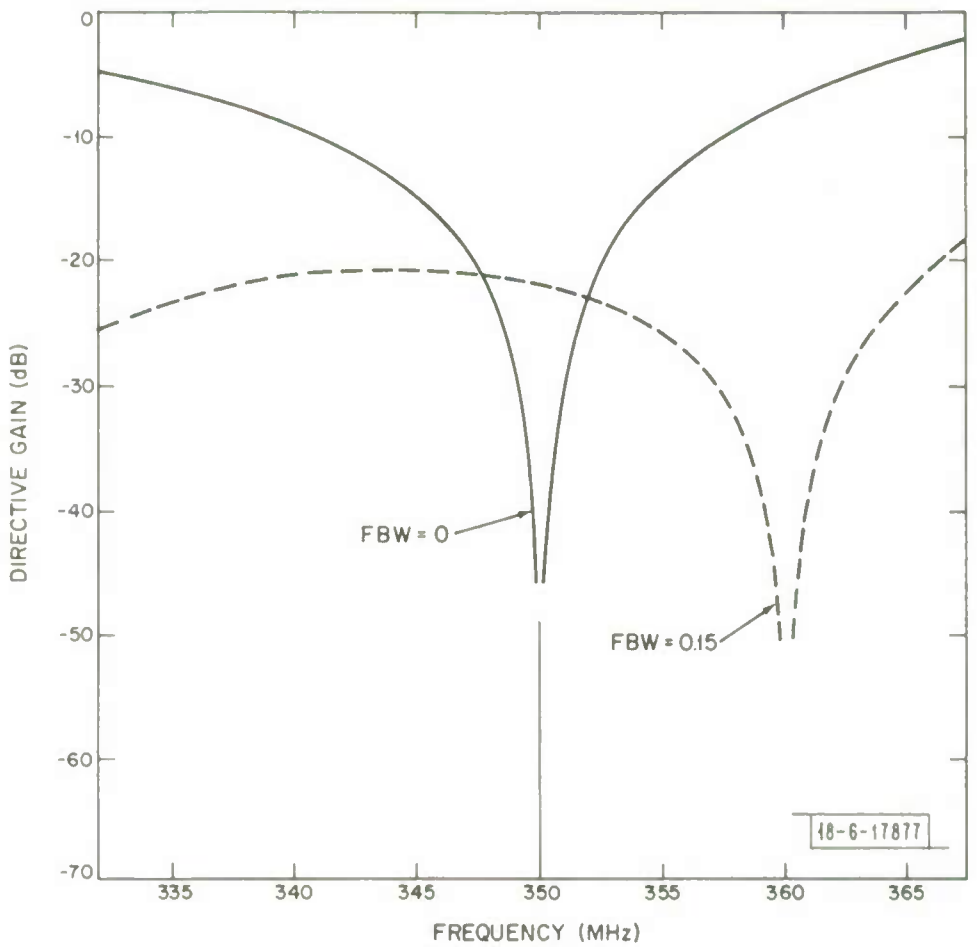

Fig. 15. Directive gain (dBi) in direction of interfering source vs frequency. $D/\lambda = 10.07$. Center frequency = 350 MHz. Source located on beam 2 maximum. Earth coverage desired radiation pattern.

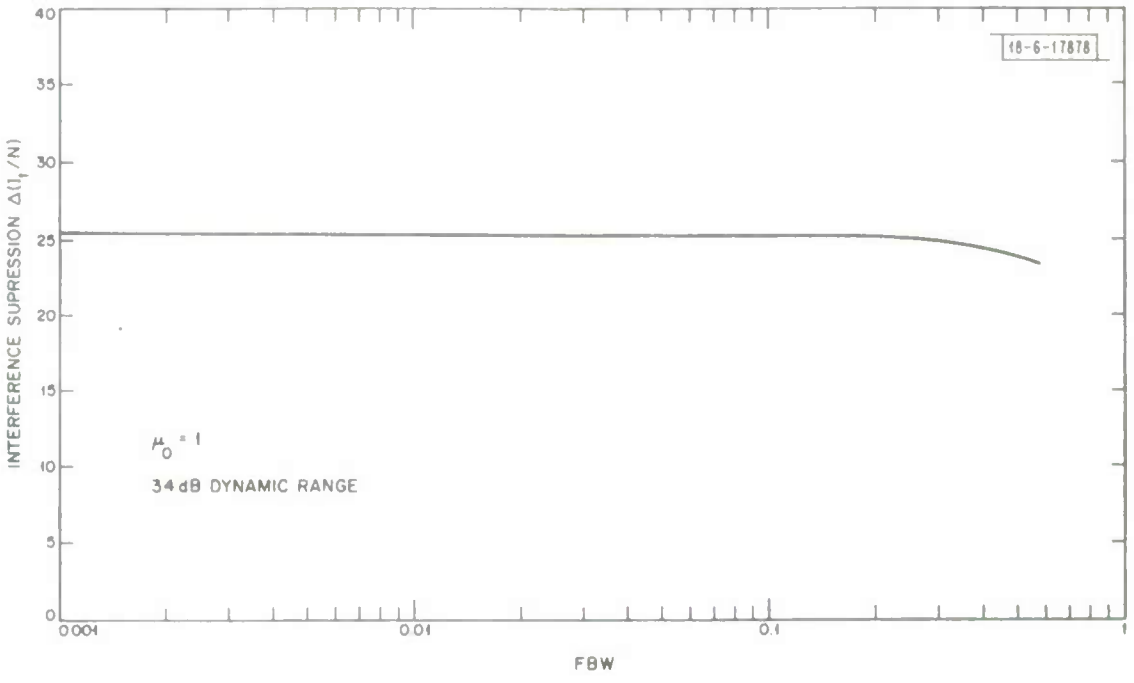

Fig. 16. Interference suppression, $\Delta(I_t/N)$, vs FBW when effective loop gain is set to unity. R_1 = 5 dB.

dynamic range and a single interfering source, R_1 = 5 dB, located at the peak of beam 2. The suppression is essentially flat for all reasonable values of FBW. The reason for this becomes evident upon examination of the eigenvalue spectrum in Fig. 14. Notice that s_2 is essentially 6-8 orders of magnitude below s_1 for small bandwidths. For μ_o = 1 and an interfering source 35 dB above thermal noise as measured at beam port 2, the changes in s_2 are well below the actual thermal noise of the system. Thus, as the bandwidth increases, the interference output power increases, but at a level well below the actual noise level of the main channel. This can be made clearer by comparing the output power for the interfering source vs FBW for the two cases μ_o = -51 dB and μ_o = 1, as illustrated in Fig. 17. Note that the variation vs frequency is essentially the same for each case; only the amplitude relative to the system thermal noise level has changed. For μ_o = 1, this amplitude remains well below the thermal noise level for all FBWs of practical interest--hence the flat characteristics of Fig. 16. For μ_o = -51 dB, the increase in interference power for increasing bandwidth is directly sensed at the output of the array; i.e., the output is relative to the effective noise level. The interference power increases approximately as the square of the bandwidth, in agreement with the results of Fig. 13. We conclude that decreasing the loop gain allows for the larger interfering sources to be minimized in the desired adaption time, but at the sake of forming a "narrowband null" on the larger sources, resulting in a somewhat greater residual output power after adaption than would occur if the algorithm were free to sense all the eigenvalues arising due to the wideband-interference. Thus the residual output power after

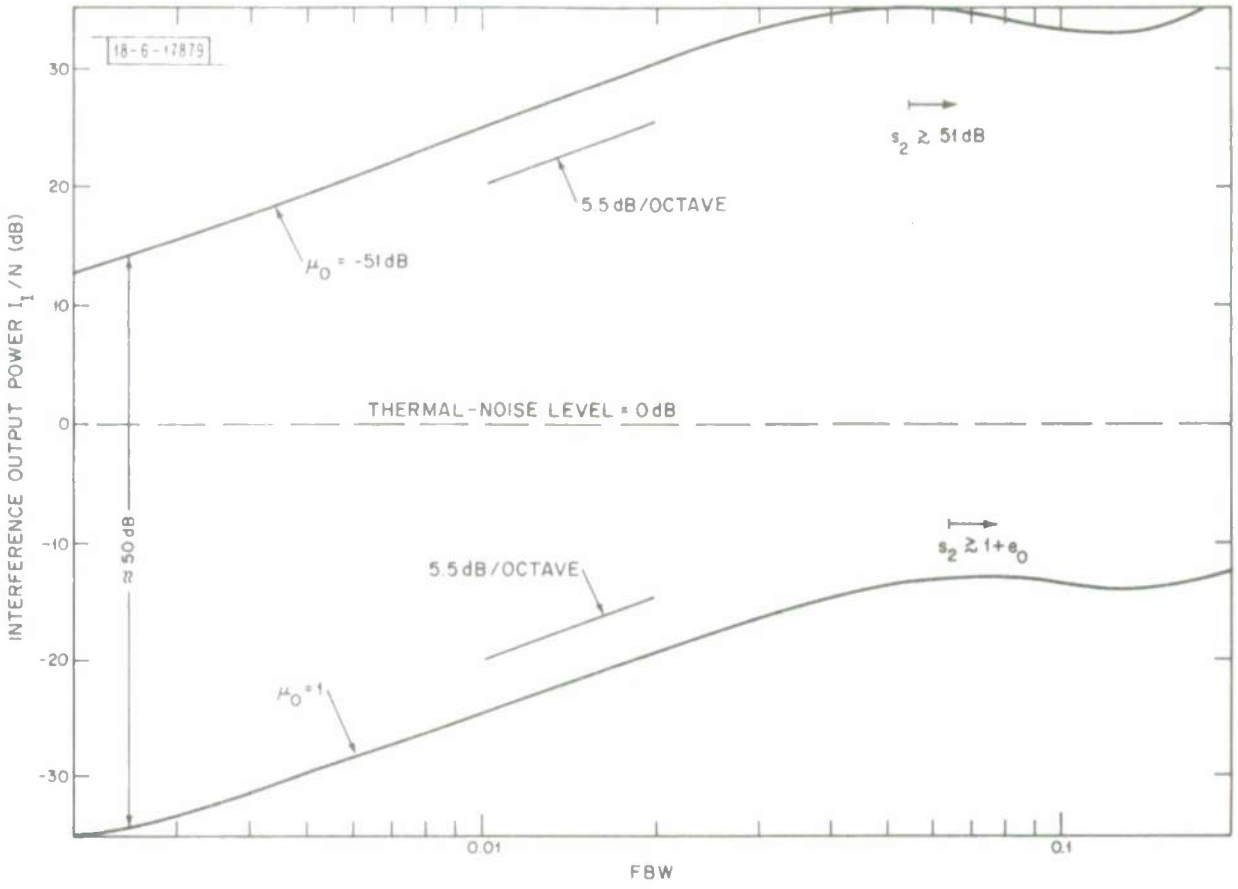

Fig. 17. Interference output power, (I_1/N), after adaption, vs FBW for $\mu_o = -51$ dB and $\mu_o = 1$. Source on beam 2 maximum. Earth coverage desired radiation pattern.

adaption increases with increasing bandwidth; hence, a limit exists as to how much one can widen the bandwidth to increase the dynamic range.

Consider now the differences in interference suppression as a function of interference location. Referring to Fig. 13, we observe that for FBW = 0, suppression of the interfering source degrades as the source moves away from a beam maximum to a position between three beams or toward the edge of the FOV. However, for FBW $\gtrsim$ .004, this trend is reversed; i.e., the suppression is best for the source located between the three beams and worst for the source at the beam peak. The reason for this can be seen as follows: The minima formed on the interfering source is essentially an FBW = 0 null. The interference output power in this case is proportional to $1/s_{MAX}$. However s_{MAX} is determined from the output power of the MBA when a maximum directivity beam is pointed toward the interference source. When the interference source location is at the peak of one of the fixed multiple beams, then s_{MAX} is maximum, given by $R_j * (4\pi A/\lambda^2)$. For the other source locations, between fixed beams of the MBA, a maximum directivity pointed toward the interference source broadens considerably, and the directivity in the direction of the interference is somewhat less than the maximum achievable directivity, $4\pi A/\lambda^2$. Thus s_{MAX} decreases for interfering sources located away from the beam peaks, and consequently a less deep null is formed on the interference. Since the adapted pattern does not change with bandwidth until FBW $\approx$ .05, the spatially broader null is inherently more broadband and interference suppression becomes best for interfering sources located away from the main beams. This behavior can be studied qualatatively by examining the ability of the MBA to form a maximum directivity beam in any desired direction.

Consider for example, the formation of a maximum directivity beam in the $\phi = 0$ plane as a function of scan angle θ_s. Selected beams are illustrated in Fig. 18, using θ_s as a parameter. Note that this plane of scan lies between beams 2 and 7. As the scan angle increases, maximum directivity available to the desired scan direction is less than the maximum 30.5 dB obtained for $D/\lambda = 10.07$, and the beam broadens considerably. Furthermore, the scanned beam maximum does not occur at the scan angle θ_s. This results in poor nulling resolution, as a ring null is then formed when the scanned maximum directivity beam is weighted with the desired pattern to form a null. The loss in directive gain to the scan direction is illustrated in Fig. 19 for three planes of scan: $\phi_s = 0$, $\phi_s = 15°$ and $\phi_s = 30°$. Results for other planes may be obtained by making use of the 30° symmetry of the seven-beam MBA geometry. Note the poorest behavior is for the $\phi_s = 0°$ plane between two beams, and as much as 5 dB loss in maximum attainable gain can occur.

Next, consider interference suppression as a function of bandwidth for a two-interfering source scenario: a large source and a weak source located in Fig. 5. The resulting $\Delta(I_t/N)$ is plotted in Fig. 20 and compared to the single source result. Note that adding the second weaker source to the single large source scenario results in a wideband, but weak suppression dominated by the weak source.

Finally we examine the nulling resolution of the MBA for the maximum signal mode of operation. We consider the two cases FBW = 0 and FBW = .0286. Define the desired-signal-to-interference ratio, (S/I_t), as the desired signal power received divided by the total interference power received where, as before, $I_t = \Sigma I_j + N$. The ability of the adaptive system to discriminate

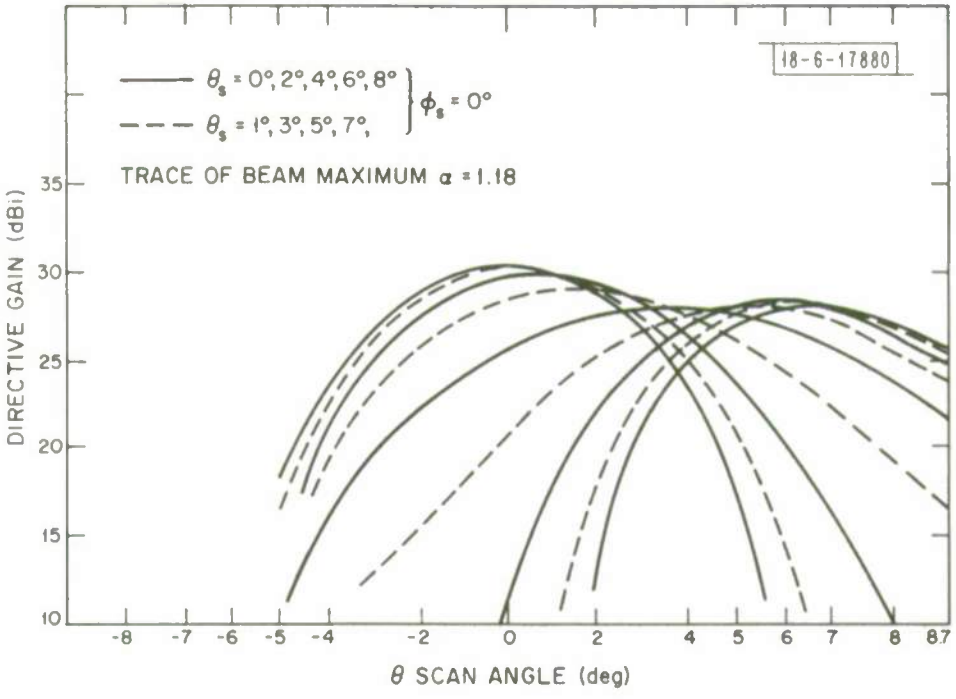

Fig. 18. Scanned maximum directivity beam radiation pattern vs scan angle θ_s in ϕ_s = 0° plane. α = 1.18 and seven beams. D/λ = 10.07.

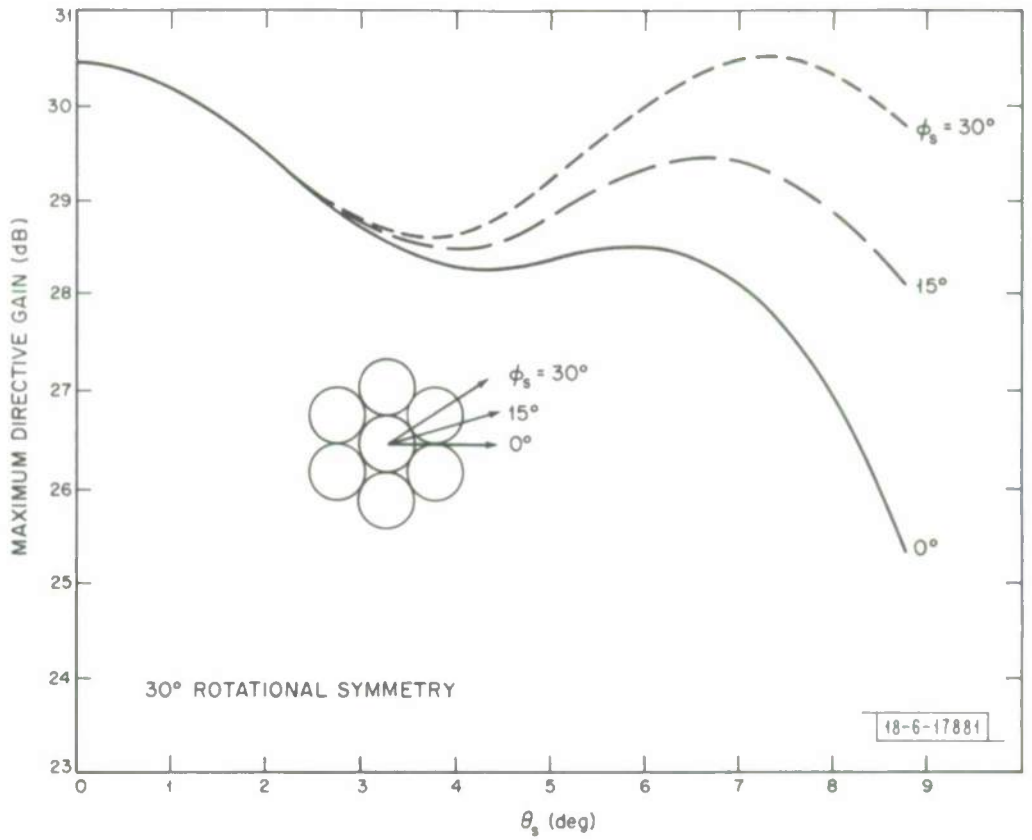

Fig. 19. Directive gain in the scan direction vs scan angle θ_s for the three planes ϕ_s = 0°, 15° and 30°. Seven beams, α = 1.18 and D/λ = 10.07.

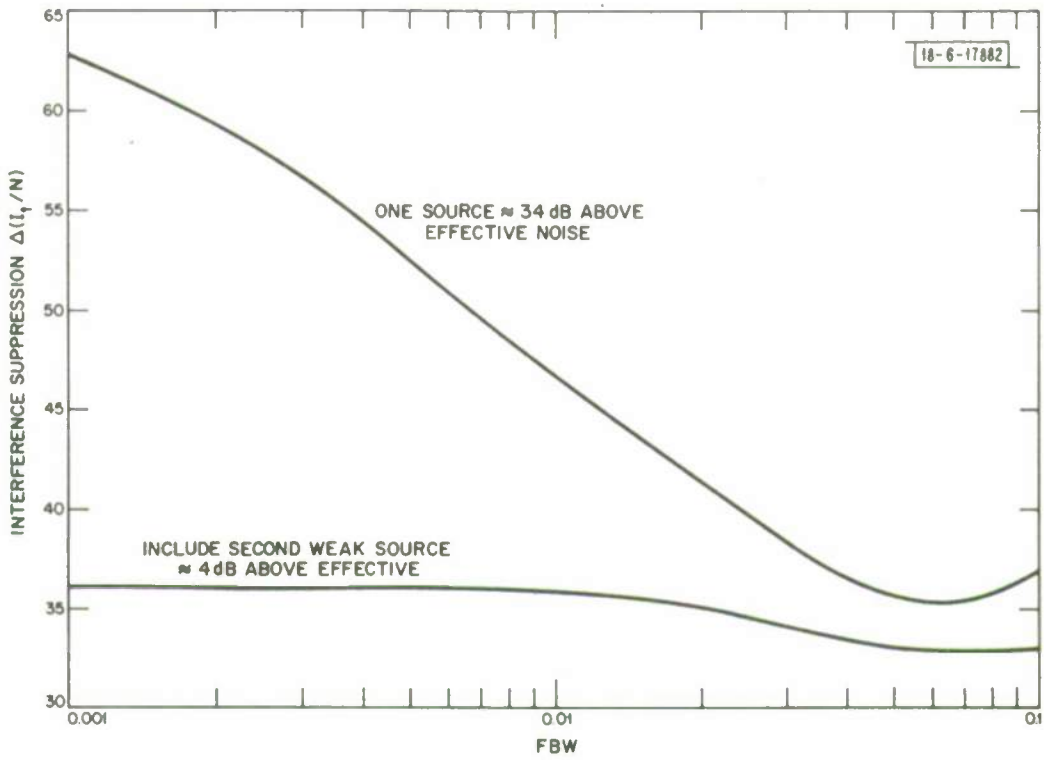

Fig. 20. Interference suppression, $\Delta(I_t/N)$, as a function of bandwidth for a single large source and two sources--one large source and a second weaker source.

between an interfering source and a signal-source can be determined from changes in (S/I_t) before and after adaption. Define the signal/interference discrimination, $\Delta(S/I_t)$, according to

$$\Delta(S/I_t) \equiv (S/I_t)_{a_{dB}} - (S/I_t)_{b_{dB}} \tag{29}$$

where the subscript "a" denotes "after adaption" and "b" denotes "before adaption". Thus $\Delta(S/I_t)$ accounts not only for the decrease in interference power after adaption, but also the decrease (or increase) of signal power due to the proximity of the desired signal to the interfering source. $\Delta(S/I_t)$ is a strong function of signal-interference-source separation. Consider for example a desired signal located at $\theta_s = 0°$, and let a large interfering source approach the signal in the $\phi = 30°$ plane. The desired pattern is a maximum directivity beam scanned to the signal source, which in this case corresponds to excitation of beam 1. Figure 21 illustrates the behavior of $\Delta(S/I_t)$ as an interfering source of strength $R_1 = 55$ dB approaches the signal for FBW = 0 and FBW = .0286, plotted vs $\Delta\theta/\theta_o$, where $\Delta\theta$ is the angular interference-signal separation, and θ_o the angular distance from the main beam to the first null of the maximum directivity radiation pattern. For $\Delta\theta = \theta_o$, the interfering source is in the null of the desired pattern; no adaption is required, so $\Delta(S/I_t) = 0$ dB. For FBW = 0, the signal-to-interference discrimination increases rapidly as the interfering source leaves the null, and then begins to decrease as the interfering signal approaches the signal. The discrimination decreases at approximately 15 dB/octave and gradually approaches 0 dB as $\theta_J \to \theta_s$. In this limiting case, no

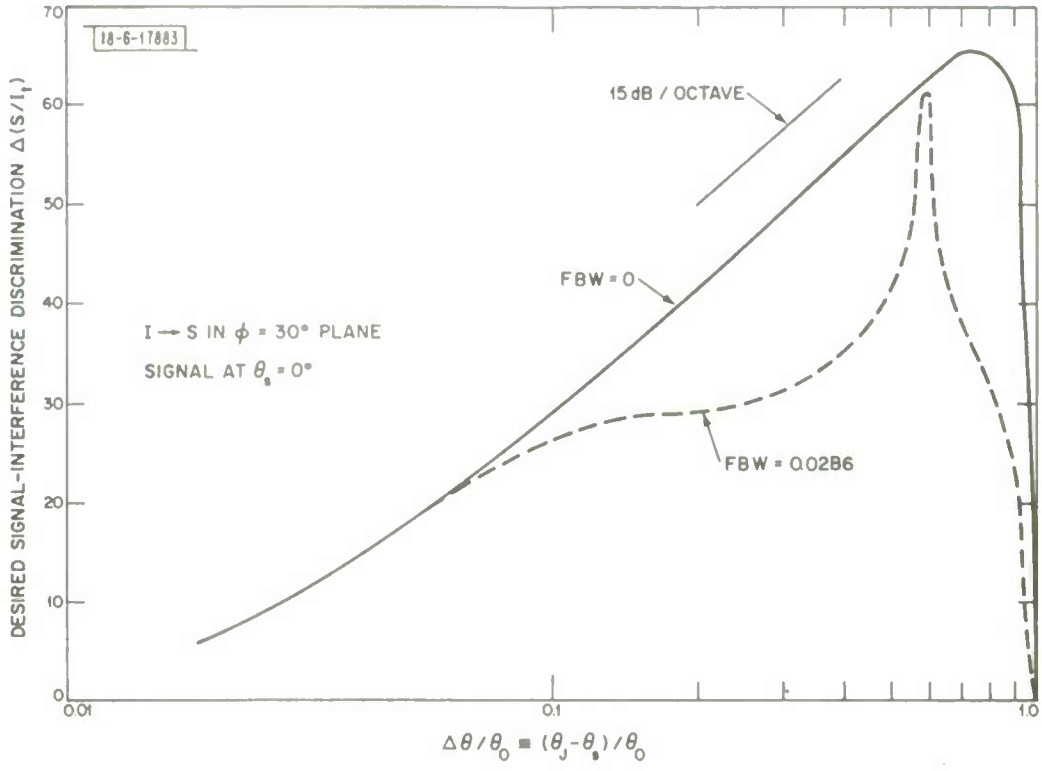

Fig. 21. Desired signal-interference discrimination, $\Delta(S/I_t)$ vs normalized signal-interference separation, $\Delta\theta/\theta_o$, for FBW = 0 and FBW = .0286. R_1 = 55 dB. Signal at θ_s = 0. I → S in ϕ = 0° plane.

discrimination can occur, and the adapted pattern is the same as the quiescent pattern. For FBW = .0286, the discrimination is much poorer. Peak discrimination occurs at $\Delta\theta \simeq 0.6\theta_o = 4°$. For the assumed geometry, this corresponds to the interfering source located between beams 1 and 2 at $\theta_J = 4°$. Note from Fig. 19 that maximum directivity for a beam scanned to $\theta_s = 4°$, $\phi_s = 30°$ is minimum, and hence we anticipate good wide-band null performance as discussed previously. Hence the high degree of interference discrimination at this point. For $\Delta\theta/\theta_o \lesssim .1$, little difference exists between the 0 bandwidth and FBW = .0286. This is in agreement with the results of Ref. 5, Fig. 10, where it is demonstrated that the effect of a wideband interfering source, relative to 0 bandwidth, becomes insignificant as $\Delta\theta \to 0$. In Fig. 22 we illustrate the loss in directivity in the signal direction (relative to $4\pi A/\lambda^2$) as the interfering source approaches the signal. The results are for FBW = 0, but are not significantly different when FBW = .0286. Since beam positioning according to $\alpha = 1.18$ was used to model the MBA, it is instructive to compare these results to beam positioning corresponding to the optimum value for α, 1.0, and also to the optimum results obtained assuming an exact replica of a scanned maximum directivity beam. Note from Fig. 25 that an improvement of approximately 3.5 dB can be achieved for $\Delta\theta/\theta_o \simeq .1$ by using optimum beam positioning.

Placement of the signal at $\theta_s = 0$ corresponds to a somewhat ideal case, so we now examine $\Delta(S/I_t)$ vs $\Delta\theta/\theta_o$ as the interfering source approaches a signal located at the edge of the field of view, in between beams 2 and 7 in the $\phi = 0$ plane. $\Delta(S/I_t)$ vs $\Delta\theta/\theta_o$ is illustrated in Fig. 23 for this case,

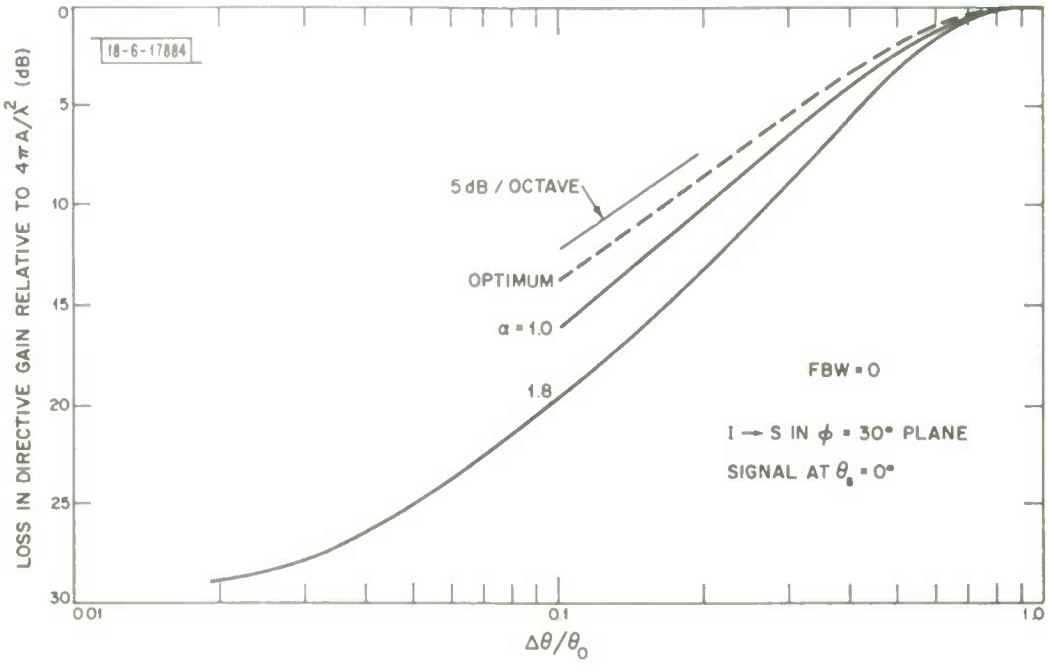

Fig. 22. Loss in directive gain as interfering source approaches desired signal in ϕ = 30° plane. Desired signal located at θ_s = 0°.

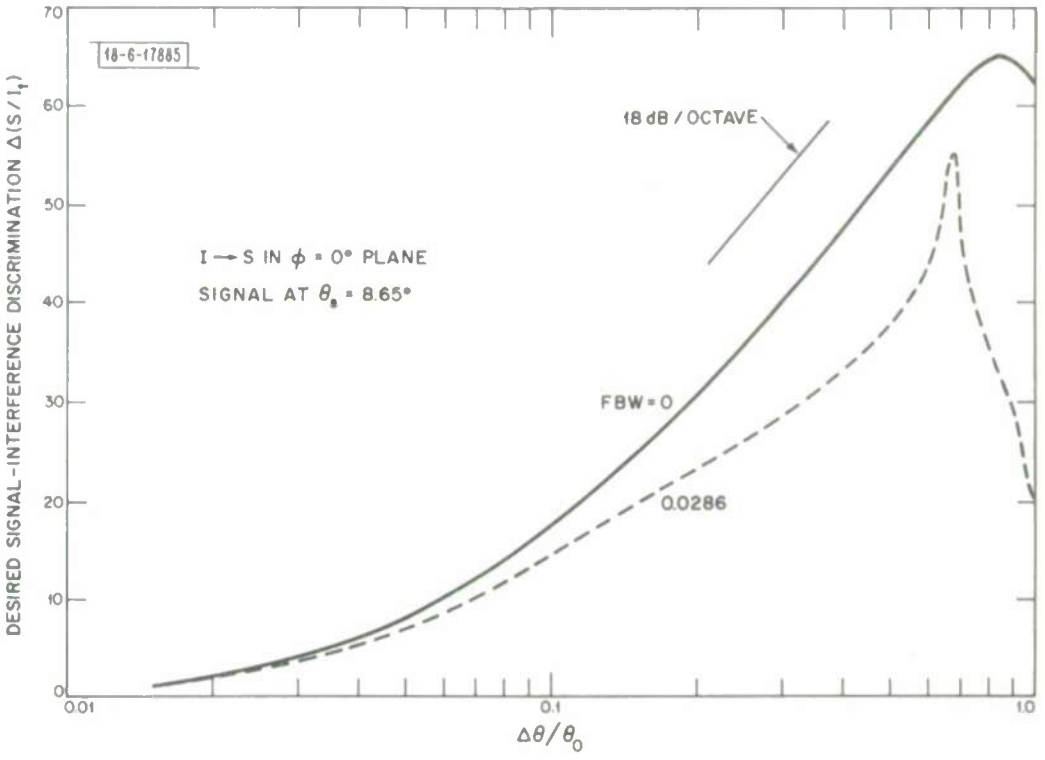

Fig. 23. Desired signal--interference discrimination, $\Delta(S/I_t)$, vs normalized signal-interference separation, $\Delta\theta/\theta_o$, for FBW = 0 and FBW = .0286. R_1 = 55 dB. Signal at θ_s = 8.65°. I → S in ϕ = 0° plane.

and the corresponding decrease in directivity in Fig. 24. Although the basic trends are similar to Figs. 21 and 22, the signal-interference discrimination has decreased significantly. The loss in directivity relative to $4\pi A/\lambda^2$ has also decreased. The curve is displaced about 5 dB down from that of Fig. 22 due to 5 dB decrease in directivity available to a signal located at the edge of the FOV at $\phi_s = 0°$, even in the absence of interference. This is evident as $\Delta\theta/\theta_o \to 1$ in Fig. 22. The relative improvement in using beam placement according to the $\alpha = 1$ has also decreased, but still yields $\approx$ 3 dB additional gain at $\Delta\theta/\theta_o \approx 0.2$.

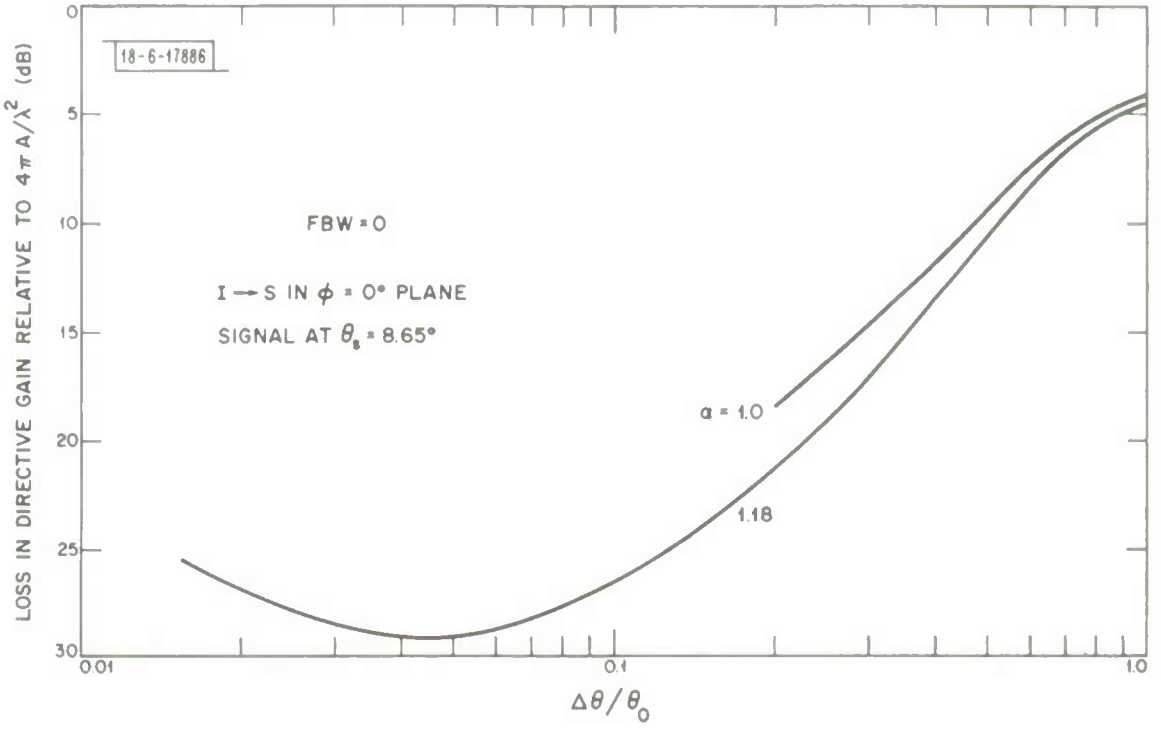

Fig. 24. Loss in directive gain as interfering source approaches desired signal in ϕ = 0° plane. R_1 = 55 dB. Signal at θ_s = 8.65°. I → S in ϕ = 0° plane.

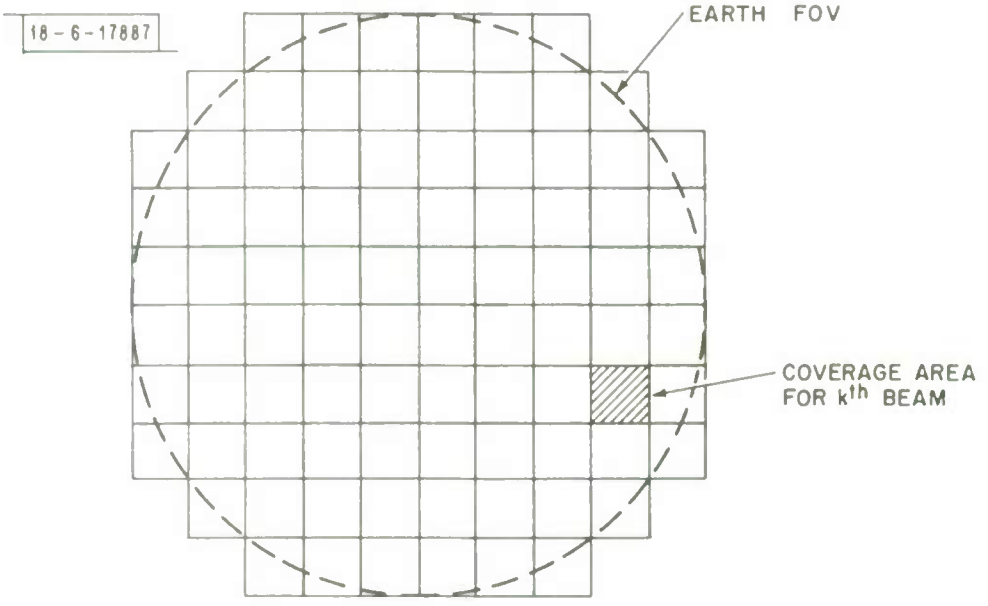

Fig. 25. Disjoint set of beams illuminating earth FOV.

V. Eigenvalue Compression Techniques

The results of the previous section have indicated the limitations on the dynamic range of power levels which can be minimized using a conventional LMS algorithm adapting on the order of a millisecond. This basic limitation arises because of the spread in the eigenvalues of the interfering source correlation matrix defined at the receive beam ports, when viewed as a function of interfering source power spread. Clearly, if one could modify the correlation matrix by appropriate changes in the algorithm after the receive beam ports, so that the modified correlation matrix exhibits a reduced spread in eigenvalues, for the same interfering-source scenario, then the algorithm could be made to operate over a wider dynamic range. From Eq. (24), the enhanced dynamic range could be used either to decrease the adaption time, decrease the nulling bandwidth or increase the dynamic range of interfering-source power levels to be minimized. Three techniques for accomplishing this compression which are particularly applicable to multiple-beam antennas will now be discussed:

(a) Pre-weighting at the receive beam ports

(b) Incorporation of a hard limiter in each element feedback loop

(c) Increasing the number of beams over a fixed field of view.

We consider the first two of these techniques in sequence, while using examples for 7, 19, 37 and 61 beams for each case in order to illustrate the latter technique.

A. Pre-Weighting at Each Receive Beam Port

One of the particular advantages peculiar to a multiple-beam antenna over an array (filled or unfilled) aperture, relative to interference cancellation, arises due to the power discrimination available from beam-port to beam-port, which is not present with the phased array. Using this power discrimination between output ports, Ricardi, et al.[6] have demonstrated, for a 19-beam system, that one can obtain a minimum of 15 dB interference rejection by simply turning off a single beam, or clusters of beams, in which the interfering sources are present. Since a power measurement at the output of each beam-port can be made very rapidly (in principle, in approximately 10/BW seconds, where BW is the bandwidth of the interference channel), the possibility of coupling this type of "pre-weighting" with a closed-loop adaptive algorithm looks promising. The rejection of the larger interfering signals is then uncoupled from the time adaption of the LMS algorithm, and the full dynamic range of the algorithm can be used to null the weaker interfering sources. This type of discrimination is strongly dependent, of course, on the degree of beam-beam coupling via the beamwidths of adjacent beams, and sidelobes of separated beams, and many possible tradeoff exist in choosing an "optimum" set of multiple beams. It is not the purpose of this section to discuss these tradeoffs, but to illustrate that the technique itself does yield a significant amount of compression for many cases. In the following we consider two specific sets of multiple beams: a very ideal set of disjoint, uncoupled beams; and a less ideal set of coupled, multiple beams corresponding to uniform aperture illumination. The former set can be

used to illustrate the best compression one could obtain using the MBA concept, and the latter offers a still ideal, but more realistic, evaluation of the compression attainable using a more practical set of multiple beams.

1. Ideal, Disjoint Multiple Beams

The particular advantages offered by a multiple-beam antenna configuration relative to pre-weighting as a means of eigenvalue compression can be illustrated by a simple example. Consider a set of beams illuminating the desired FOV which are spatially disjoint from each other--i.e., each beam's radiation pattern is non-zero only over its localized coverage area over the FOV, and is zero when evaluated at the coverage area of any of the other beams. The radiation patterns of such an idealized set of beams covering the earth FOV might appear as in Fig. 25. If we define $\psi_k(\theta)$ to be the radiation pattern of the kth beam, then $\psi_k(\theta) = 0$ unless θ occurs over the coverage area of the kth beam. In this case we normalize $\psi_k(\theta) = 1$. Consider then, two interfering signals having power levels I_1 and I_2 positioned in beams 1 and 2, respectively. The interfering-signal correlation matrix $\underline{\underline{R}}$, assuming zero bandwidth signals and normalizing to thermal noise level N is then given by

$$\underline{\underline{R}}_{k,q} = (I_1/N)\ \psi_k(\theta_1)\ \psi_q^*(\theta_1) + (I_2/N)\ \psi_k(\theta_2)\ \psi_q^*(\theta_2) + \delta_{k,q} \qquad (30)$$

where $\delta_{k,q} = 0$, $k \neq q$; $\delta_{k,q} = 1$, $k = q$. Noting the disjoint properties of the beams, then $\underline{\underline{R}}$ must take the diagonal from

$$\underline{\underline{R}} = \begin{bmatrix} \frac{I_1}{N} + 1 & & & 0 \\ & \frac{I_2}{N} + 1 & & \\ & & 1 & \\ & & & \ddots \\ 0 & & & 1 \end{bmatrix} \tag{31}$$

Denote the eigenvalues of $\underline{\underline{R}}$ by s_k, $k = 1,\cdots,K$, as defined in Eq. (15). Then from Eq. (31), $s_1 = \frac{I_1}{N} + 1$, $s_2 = \frac{I_2}{N} + 1$, $s_3 = \cdots, s_k = 1$, and the eigenvalue spread due to the interfering sources is approximately I_1/I_2, assuming $I_1 > I_2$. The loop time constants, $\tau_1,\cdots,\tau_K$, can be expressed in terms of the s_k according to:

$$\tau_k = \frac{\tau}{1 + \mu_o (1 + s_k)} \tag{32}$$

where μ_o is the effective loop gain. Hence, assuming s_1, $s_2 >> 1$, the dynamic range of adaption times for the two sources under consideration is given by $\tau_2/\tau_1 = I_1/I_2$.

Consider now pre-weighting at each of the beam ports as illustrated in Fig. 26. It is clear that, due to the disjoint properties of the K multiple beams, interfering signal I_1 can be reduced independently by simply controlling A_1 and similarly I_2 can be reduced by simply controlling A_2. Assuming A_1 and A_2 are set as desired, then the correlation matrix $\underline{\underline{R}}'$after pre-weighting

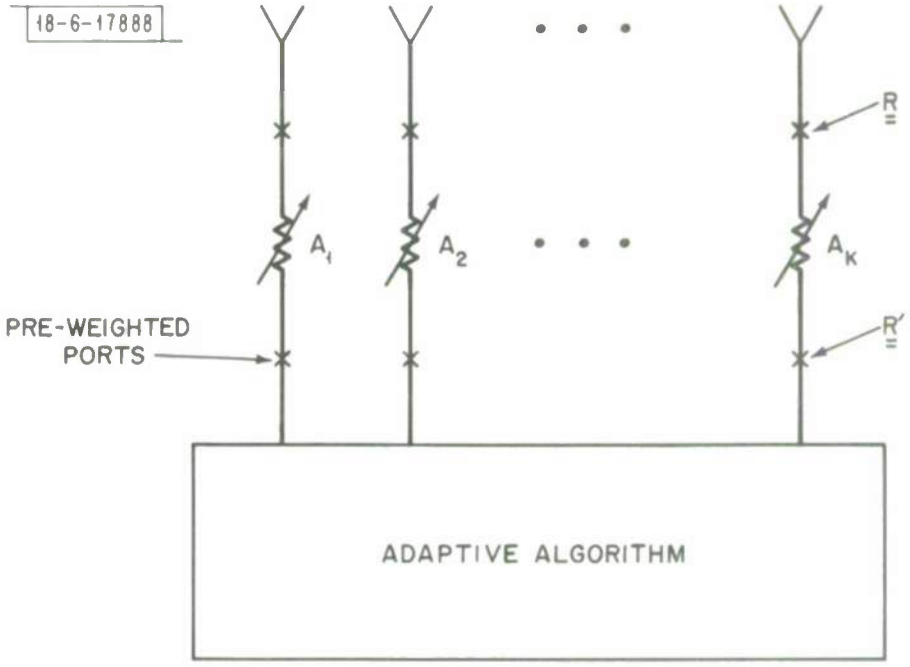

Fig. 26. Pre-weighting at each of the MBA beam ports.

takes the form

$$\underline{\underline{R}}' = \begin{bmatrix} |A_1|^2\left(\frac{I_1}{N_o} + 1\right) & & & 0 \\ & |A_2|^2\left(\frac{I_2}{N_o} + 1\right) & & \\ & & 1 & \\ & & & \ddots \\ 0 & & & & 1 \end{bmatrix} \tag{33}$$

and the compressed dynamic range of eigenvalues is given by

$$\frac{\tau_2'}{\tau_1'} = \frac{|A_1|^2}{|A_2|^2}\ \frac{I_1}{I_2} \tag{34}$$

Clearly A_1 and A_2 can be chosen so that $\tau_2'/\tau_1' << \tau_2/\tau_1$.

In the general case, pre-weighting occurs at several ports, and a systematic scheme for choosing the pre-weights at the kth port must be defined. We adopt the following scheme: Define s_{MAX} to be the maximum power level anticipated out of any of the beam ports in the absence of pre-weighting, and A_k to be the value of pre-weighting desired at the kth port. The average power measured at the kth port in the absence of pre-weighting is $R_{k,k}$. Define A_o to be the maximum value of pre-weighting allowed and P_M the maximum output power allowed at the output of any of the beam ports after pre-weighting. Then $A_o = s_{MAX}/P_M$. If a source appears at the kth beam port at a level greater than P_M, we adjust A_k to bring the level down to P_M. If the

source appears at a level less than P_M, we do no pre-weighting at that port. Thus large jammers appearing at the kth beam ports will be initially reduced by A_k before adaption begins; smaller jammers will not be affected. Hence the spread in eigenvalues at the terminals defined after pre-weighting should be smaller than those defined at the terminals before pre-weighting. This modified correlation matrix $\underline{\underline{R}}'$ after pre-weighting is then given by

$$\underline{\underline{R}}'_{k,q} = A_k \, \underline{\underline{R}}_{k,q} \, A_q \tag{35}$$

where we assume the A_k will all be real (i.e., simple attenuators). The eigenvalues $\{s_k'\}$ of $\underline{\underline{R}}'$, and hence the compressed dyanmic range τ_2'/τ_1', can be controlled as desired by properly choosing P_M (or A). Using the above reasoning, the A_k are given by

$$A_k = \begin{cases} 1 \quad , & R_{k,k} < P_M \\ \sqrt{\dfrac{P_M}{R_{k,k}}} \quad , & R_{k,k} > P_M \end{cases} \tag{36}$$

Using this technique, the amount of compression attainable for a fixed amount of pre-weighting can be estimated. For the two-interfering signal case, the spread in eigenvalues before pre-weighting is I_1/I_2. Assuming $I_1 >> I_2$, the spread in eigenvalues after pre-weighting is $A_1 \, I_1/I_2$. We define the compression parameter C for the two-signal case according to

$$C \equiv \frac{(s_1/s_2)_{dB} - (s_1'/s_2')_{dB}}{(s_1/s_2)_{dB}} \tag{37}$$

Thus, optimum compression for the above example is given by

$$C = (A_1)_{dB} / (I_1/I_2)_{dB} \tag{38}$$

Thus 100% compression is obtained when $(A_1)_{dB}$ is equal to the dynamic range of power levels of the interfering sources.

B. Coupled Multiple Beams

Clearly, the basis for the above eigenvalue compression scheme depends on the degree that one can approximate the ideal set of disjoint multiple beams postulated above. In the practical application, one usually generates a set of beams which are spatially orthogonal (i.e., they satisfy the property

$$\int_{\text{all space}} \phi_k(\theta,\phi)\, \phi_q(\theta,\phi)\, \sin\theta d\theta d\phi = \begin{cases} 0, & k \neq q \\ 1, & k = q \end{cases} \tag{39}$$

where $\phi_k(\theta,\phi)$, $k = 1,\cdots,K$, denotes the beam patterns) or nearly so, but not disjoint. Examples of such beams are the orthogonal set of $\sin(x-x_k)/(x-x_k)$ beams for a linear array, where the x_k denote the beam positions, and $J_1(x-x_k)/(x-x_k)$ for a two-dimensional aperture, where $J_1(x)$ is the first order Bessel function. In this case adjacent beams overlap at a given cross-over level, usually between 3 and 4 dB, and beams further apart are coupled by the relative sidelobe levels of each beam. Thus the correlation matrix at the receive beam ports is not diagonal, but generally consists of decreasing off diagonal elements, depending on the actual spread in interference power levels. However, we show that the general trends described above still hold, and a significant amount of compression can be obtained for certain

interfering-source scenarios.

In order to illustrate these effects for a more practical MBA beam configuration, we utilize the basic beam geometry discussed in Section II. Before analyzing in detail the degree of eigenvalue compression one can obtain by pre-weighting at the beam ports, recall the simple two-source example treated in Section III, Figs. 3-5, having R_1 = 55 dB and R_2 = 25 dB relative to 0 dB antenna gain, as shown in Fig. 3. The corresponding eigenvalue spread for this case is illustrated in Table 3 under the heading "Conventional LMS Algorithm". Note that, for the two assumed sources, there are three significant eigenvalues having a spread s_1/s_3 = 40.1 dB. Since the interfering sources are separated by more than a few beamwidths (beamwidth here refers to the beamwidth of a maximum gain beam available from the aperture), eigenvector $\underline{e}_1$ corresponding to s_1 yields the best approximation to a maximum gain beam scanned to the position of I_1, yielding $s_1 \simeq 85$ dB (i.e., $s_1 \simeq \frac{I_1}{N} * 4\pi A/\lambda^2$). Note that since I_1 occurs on a beam peak, the gain in the direction of I_1 is essentially $4\pi A/\lambda^2 \simeq 30.5$ dB. Similarly, $\underline{e}_2$ corresponds to pointing a scanned maximum gain beam in the direction of I_2. However, since I_2 occurs between beams, there is approximately 1.5 dB loss in gain due to scanning the beam to I_2, which is reflected in a value for s_2 somewhat lower than the expected 55.5 dB. The third eigenvalue s_3 arises due to the bandwidth spread of the interfering source about the null formed on I_1. The time adaption of I_1/N and I_2/N is illustrated in Fig. 4 and has been discussed in detail in Section III. Recall that, since the system only senses a 34 dB dynamic range in interference power, the third eigenvalue s_3 is not sensed, and the adapted

Table 3

Eigenvalue Distribution for Interference Sources in Fig. 3.
Seven Beams, $D/\lambda = 10.7$, FBW = .0286

Eigenvalue Distribution for Two-Jammer Case (10 MHz BW)

Eigenvalue	Conventional LMS Algorithm	20 dB Pre-weighting	Hard-Limiting	Hard-Limiting + Pre-Weighting
s_1 (dB)	85.5	67.6	86.2	72.5
s_2	53.5	53.2	68.9	61.2
s_3	45.4	44.0	60.1	50.7
s_4	13.1	13.0	27.1	19.7
s_5	6.8	6.5	22.4	14.5
s_6	1.1	1.1	17.4	9.0
s_7	1.1	0.9	15.2	7.8
	s_1/s_3 (dB)	s_1/s_3 (dB)	s_1/s_3 (dB)	s_1/s_3 (dB)
	40.1	23.6	26.2	21.2

level of I_1 is quite large. Similarly, source I_2 is sensed as a "weak" source relative to μ_o, and is consequently reduced only slightly.

Consider now introducing a maximum of 20 dB pre-weighting at each beam port according to the scheme outlined in Eq. (36). Since $s_{MAX} \simeq 85$ dB, $P_M = 65$ dB, and hence interfering sources appearing at any beam port at a level higher than 65 dB are reduced accordingly. For the case considered, I_1 appears at port 2 at a level of 85 dB, and 20 dB pre-weighting is introduced at this port before adaption begins. No pre-weighting occurs at the other ports due to the inherent MBA discrimination between beams (each beam has a 17-dB first sidelobe level). The corresponding eigenvalue spread using $\underline{\underline{R}}'$ for this case is tabulated in Table 3 under the head "20 dB maximum pre-weighting". The compression in eigenvalues is clearly evident: from 40.1 dB to 23.6 dB. In order to fully realize the benefits of this spread, the effective loop gain μ_o must be set to correspond to the decreased $s'_{MAX} = 67.6$ dB. Later we show that the variation in s'_{MAX} vs interfering source positioning is small, and a value of $\mu_o = -38$ dB can be determined from the highest attained value of s'_{MAX} when averaged over many source scenarios. Using this value of μ_o, the corresponding time adaption of I_1/N and I_2/N is illustrated in Fig. 27, along with the adapted radiation pattern in Fig. 28. Note that at $t = 0$, the power level of I_1 has been initially reduced $\simeq 23$ dB by the pre-weighting and the adapted output power has been reduced considerably, as is evident by the deeper null formed on I_2 as compared to the no-pre-weighting case. The 23.6 dB spread in eigenvalues is more than adequately handled by the 34 dB dynamic range sensitivity of the loops.

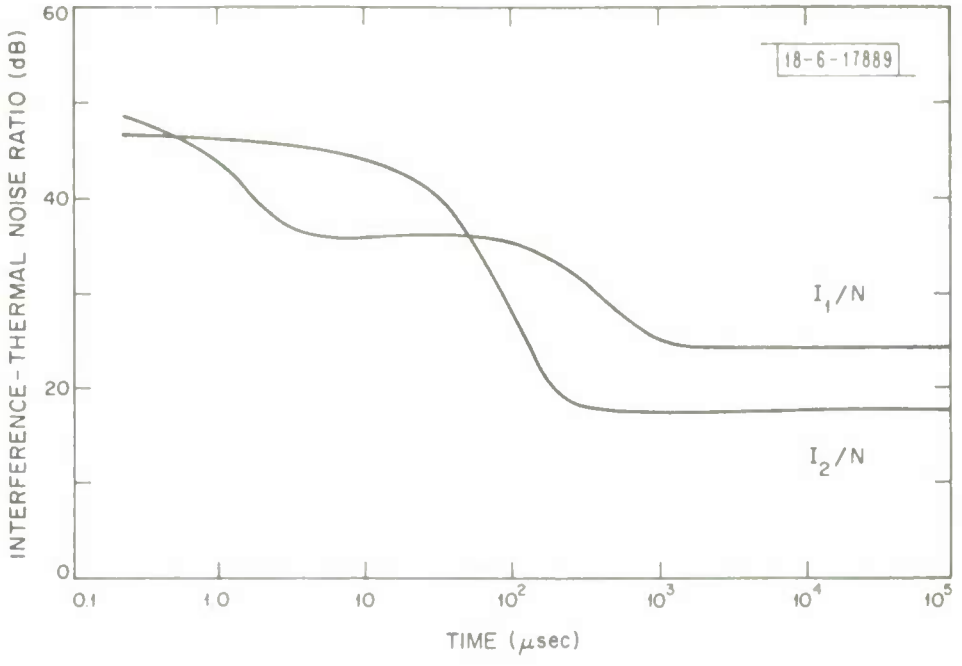

Fig. 27. Interference-thermal noise ratio vs time using 20 dB maximum pre-weighting at each beam port. Two-source interference scenario of Table 2.

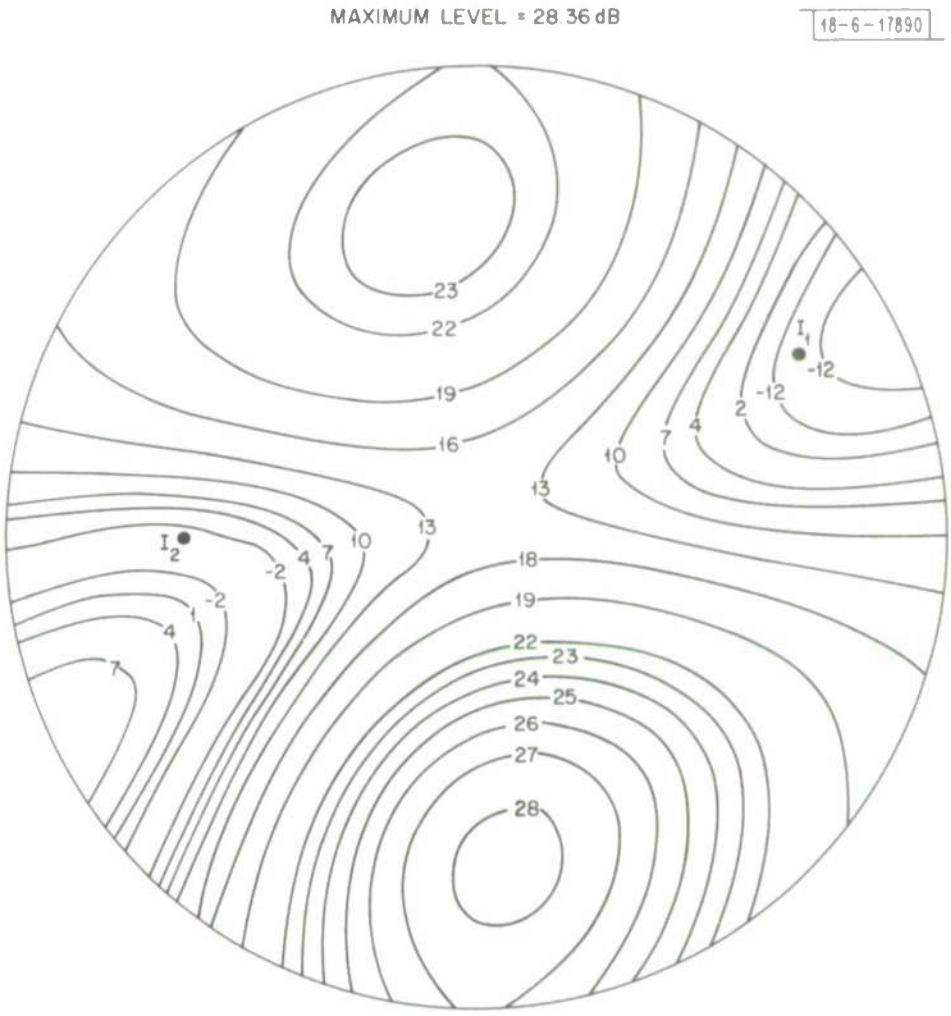

Fig. 28. Adapted radiation pattern using 20 dB pre-weighting at each beam port. Two-source interference scenario of Table 2.

The results obtained in the above example were perhaps optimistic in the sense that only two interfering signals which were widely separated were present. A much more realistic evaluation of the technique would be to consider a variety of interfering sources, having varying power levels and located somewhat randomly over the FOV. We consider three such cases as listed in Table 4 below:

Table 4

Case	Interfering Sources	Power Levels R_j (dB)
1	6	55, 45, 40, 35, 30, 25
2	2	55, 25
3	6	55, 45, 45, 45, 45, 45

Each scenario is assumed dominated by a single large interfering source having $R_1 = 55$ dB. Case 1 consists of six scenarios spread somewhat uniformly in power over a 30 dB range; Case 2 consists of a weak and a strong source; and Case 3 consists of six sources, but with only a 10 dB spread in power levels. For each case, the amount of compression and maximum eigenvalue of $\underline{\underline{R}}'$ will be averaged over 10 different scenarios generated randomly over the FOV, as a function of the pre-weighting parameter A_o according to the pre-weighting scheme defined in Eq. (36). It is important to ascertain the value of s'_{MAX} after pre-weighting so that the effective loop gain can be properly set. Since variations in s'_{MAX} are small, the loop gain can then be set using the largest value obtained over many random scenarios. Each case will be considered for zero bandwidth, and a 10 MHz bandwidth at 350 MHz. For zero bandwidth, the spread in dominant eigenvalues is given by s_1/s_J, where

J is the number of interfering sources. The remaining eigenvalues are all at the thermal noise level and correspond to thermal noise power at the output when linear combinations of their eigenvectors are used as weights. For the 10 MHz bandwidth, we use s_1/s_{J+1} as a measure of the eigenvalue spread, accounting for the added degree of freedom used up by the non-zero bandwidth. The results for 7, 19, 37 and 61 beams will be considered for each of the cases enumerated above.

1. Case 1--BW = 10 MHz (2.9%)

The eigenvalue compression for seven beams is illustrated in Fig. 29, where we plot s_1/s_{J+1} (10 MHz bandwidth) vs the scenario under consideration using pre-weighting parameter A_o as a parameter. Observe that as A_o increases, the spread in eigenvalues consistently decreases, although the effect is less significant for some scenarios. A saturation point is reached, where increasing A_o further does not yield further compression. At this point, increasing A_o results in setting an additional attenuation which is the same for each loop, resulting in a loss in interference and noise power output, but not changing I/N. This transition region is a function of the beam coupling and number of interfering sources, and does not occur for the ideal disjoint set of beams. We note however, that for A_o = 20 dB, a significant amount of compression can be realized even for a seven-beam system and six interfering sources operating over a 3% bandwidth.

Results similar to those illustrated in Fig. 29 were also run for 19 and 37 beams, and are summarized in Table 5. In the table, we tabulate the average of s'_{MAX} and s_1/s_{J+1} over the 10 random scenarios, along with the

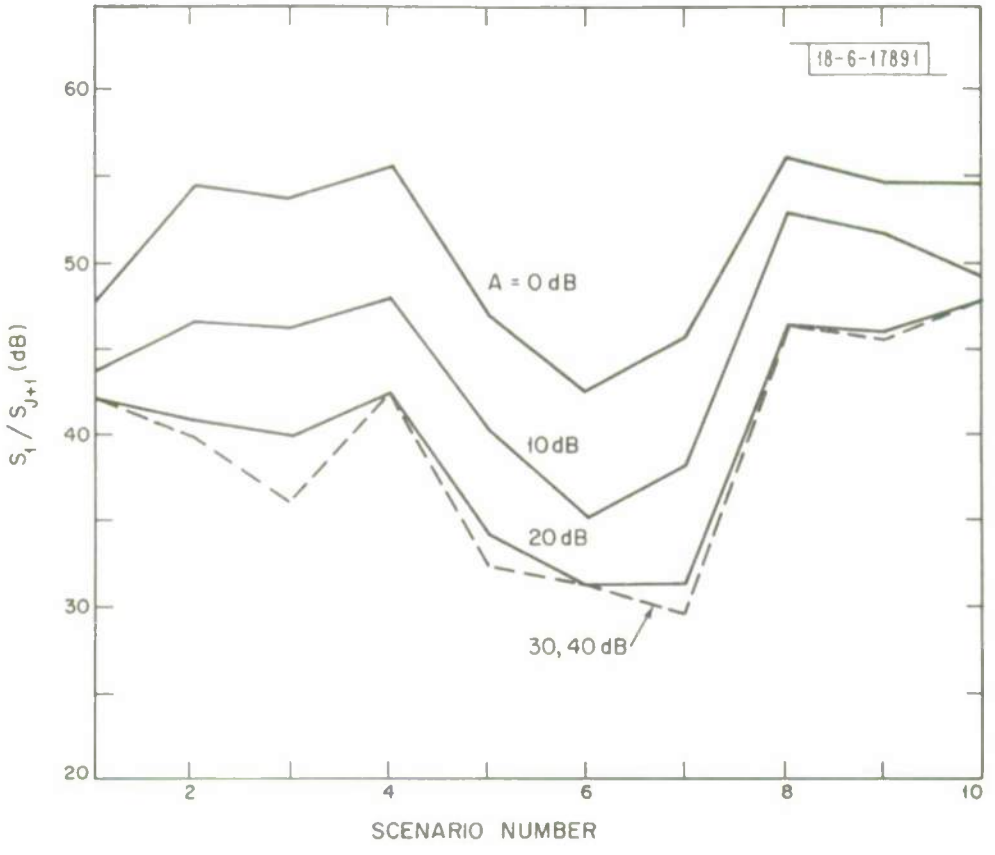

Fig. 29. Eigenvalue spread s_1/s_{J+1} vs scenario number for Case 1, Table 4. Each scenario equals six sources randomly located over the FOV. FBW = .0286.

percent eigenvalue compression C defined in Eq. (8), as a function of pre-weighting A_o. For comparison purposes, the same 10 random scenarios were used for each row of the table. As A_o increases in 10 dB steps, $(s'_{MAX})_{AV}$ gradually decreases until a point is reaches where a further increase in A_o results in a corresponding decrease in $(s'_{MAX})_{AV}$ by the same amount; no further compression is obtained. This transition occurs quite rapidly for seven beams, but larger values of A_o could be used as the number of beams increases or the number of interfering sources decreases. Note also, that increasing the number of beams, for a fixed number of interfering sources, in itself yields significant eigenvalue compression. This can be explained as follows: For a given interfering source separation, increasing the number of beams corresponds to a larger source separation in terms of antenna beamwidths, since the antenna diameter is increased to attain a narrower beamwidth in order to cover the fixed FOV. In the limiting case of a very large number of beams, and no pre-weighting, a maximum gain beam is formed on each interfering source, and is essentially uncoupled from the other sources. In this limiting case, these beams are then the eigenvector beams, and hence, at least for zero bandwidth, the eigenvalues then span exactly the range of power levels of the interfering sources. Thus for zero bandwidth, and a 30 dB spread in interference source power levels, we expect the spread $s_1/s_J \rightarrow 30$ dB as the number of beams increases. This general trend can be seen in Table 5 for a 3% bandwidth. In Table 6, we repeat the results of Table 5 at zero bandwidth, where the above trends are even more evident. For a fixed number of beams, pre-weighting adds an additional amount of compression, which averages

Table 5

Eigenvalue Compression vs Maximum Pre-Weighting A for Case 1.
Six Interfering Sources R_j = 55, 45, 40, 35, 30, 25 dB.
FBW = .0286. Ten Cumulative Averages.

No. of Beams	A_o	$(s'_{MAX})_{AV}$	$(s'_1/s'_{J+1})_{AV}$	Compression (%)
7 Beams (D/λ = 10.7)	0	84.2 dB	51.3 dB	0
	10	77.8	45.2	11.9
	20	70.7	40.3	21.4
	30	61.5	39.5	23
19 Beams (D/λ = 16.1)	0	88.4	35.2	0
	10	84.3	35.1	8.8
	20	77.9	30.9	19.7
	30	69.7	28.3	26.5
37 Beams* (D/λ = 25)	0	91.6	35.2	0
	10	----	----	----
	20	82.4	27.2	22.7
	30	75.4	23.6	33.0

*Eight Cumulative Averages

Table 6

Pre-Weighting Compression for Case 1--7, 19, 37 and 61 Beams--
FBW = 0. Ten Cumulative Averages

No. of Beams	A	$(s'_{MAX})_{AV}$	$(s'_1/s'_{J+1})_{AV}$	Compression (%)
7	0 dB	84.2 dB	48.3 dB	0
	10	78.0	42.6	11.8
	20	70.7	38.3	20.7
	30	61.5	36.9	23.6
19	0	88.4	34.3	0
	10	84.3	31.3	9.6
	20	77.9	28.3	17.5
	30	69.7	26.7	22.2
37	0	91.8	32.1	0
	10	87.6	28.2	12.2
	20	82.5	24.8	22.8
	30	75.5	22.6	29.5
61	0	94.2	31.6	0
	10	----	----	----
	20	84.4	23.8	24.7
	30	78.4	22.5	28.2

about 25% when referred to the "no pre-weight" result. If one contrasts, for example, a seven-beam system with no pre-weighting to a 19-beam system with pre-weighting, a 45% compression can be obtained for a 3% bandwidth.

Case 1 represents somewhat of a "worst case" for a seven-beam system and it is of interest to compare these results to the somewhat less restrictive interference scenario of Case 2 and 3. Results for these two cases are summarized in Tables 7 and 8, respectively, at zero bandwidth. Since Case 2 assumes there are only two interfering sources randomly located over the FOV, the sources are on the average separated more than a beamwidth, and hence the eigenvector beams are nearly uncoupled, leading to $(s_1/s_J)_{AV}$ approaching 30 dB even for seven beams. The degree of compression, C, is larger than Case 1, averaging near 40% using A_o = 30 dB for either 7, 19, 37 or 61 beams. In Case 3, we consider six interfering sources, but spread only 10 dB in power level, where five sources have a value for R_j = 45 dB. Hence for seven beams a large eigenvalue spread arises when no-pre-weighting exists, since some sources will necessarily lie close together (measured in antenna beamwidths); for 19-61 beams the eigenvalue spread is much closer to the anticipated 10 dB spread. The amount of compression realized is larger where the initial spread before pre-weighting is large, but decreases as the initial spread decreases.

C. Hard Limiter in Element Feedback Loop

One means for alleviating the drawbacks of the power response characteristics of the conventional LMS adaptive algorithm has been to modify each adaptive loop by incorporating a hard-limiter in the element branch feeding

Table 7

Eigenvalue Compression vs Pre-Weighting A for Case 2.
R_j = 55, 25 dB. Ten Cumulative Averages.

No. of Beams	A	$(s'_{MAX})_{AV}$	$(s'_1/s'_J)_{AV}$	Compression (%)
7	0	84.2 dB	32.4 dB	0
	10	77.6	26.5	18.2
	20	71.3	21.5	33.7
	30	63.1	17.6	45.7
19	0	88.5	30.4	0
	10	83.0	25.3	17.5
	20	77.6	21.2	30.2
	30	70.5	19.2	36.8
37	0	91.7	30.5	0
	10	87.9	27.0	11.5
	20	83.1	22.9	24.8
	30	76.7	20.3	33.5
61	0	94.2	30.4	0
	10	----	----	----
	20	84.6	21.2	30.2
	30	79.1	17.9	41.0

Table 8

Eigenvalue Compression vs Pre-Weighting A for Case 3.
R_j = 55, 45, 45, 45, 45, 45. Ten Cumulative Averages.

No. of Beams	A	$(s_{MAX})_{AV}$	$(s_1/s_J)_{AV}$	Compression (%)
7	0	84.4 dB	35.3 dB	0
	10	78.3	29.6	16
	20	69.8	24.8	29.8
	30	60.3	24.0	32.0
19	0	88.5	18.9	0
	10	84.3	16.0	10.5
	20	77.3	15.6	17.5
	30	68.3	15.9	15.9
37	0	91.9	15.4	0
	10	87.9	11.7	24
	20	82.1	12.1	21.4
	30	74.4	12.2	20.8
61	0	64.3	14.4	0
	10	----	----	----
	20	84.3	10.3	28.5
	30	77.8	10.4	27.8

back from the beam port to the correlator. The effects of such a modification have been examined in Refs. 1 and 7, where it is concluded that the hard-limiter modification does not affect the spread in eigenvalues, but can be used to compress the dynamic range of feedback voltages existing in the adaptive loop. However, the basis of these analyses assumes an array antenna geometry, where the power output of each array element is identical, regardless of the number and level of interfering sources. Thus the effect of the hard-limiting is the same for each port, and the correlation matrix obtained using hard-limiting is modified only by the hard-limiting output constant h; hence all eigenvalues are similarly modified. Thus, although the individual values of the eigenvalues are modified, they are all changed by the same amount so that no compression occurs. However, use of the hard-limiter with an MBA eliminates these drawbacks, and we shall see that, theoretically, up to 50% compression can be obtained using this modification.

The modified correlation matrix, $\underline{\underline{R}}'$, obtained using a hard-limiter in the element feedback loop has been derived by Brennan, et al.[7] for gaussian, ergodic inputs and omni-directional antenna elements. Assuming narrowband interference, $\underline{\underline{R}}'$ can be expressed in the form[1]

$$\underline{\underline{R}}' = \frac{h}{\sqrt{R_{k,k}}} \underline{\underline{R}} \tag{40}$$

where h is the hard-limiter output, $R_{k,k}$ the average power out of the kth port and $\underline{\underline{R}}$ the correlation matrix in the absence of hard-limiting. Equation (40) can be shown to be valid for antenna ports which are non-omni-

directional--e.g., the MBA. For the array geometry employing omni-directional elements, $R_{1,1} = R_{2,2} = \cdots = R_{K,K}$, so that (40) differs from $\underline{\underline{R}}$ by a constant, leading to the same eigenvalue spread with and without hard-limiting. However, for the MBA, $R_{k,k}$ varies from beam port to beam port, so that $\underline{\underline{R}}'$ has a different eigenvalue spread than $\underline{\underline{R}}$.

The degree of eigenvalue compression obtained using $\underline{\underline{R}}'$relative to $\underline{\underline{R}}$ can be estimated using the disjoint set of ideal beams introduced previously. For interfering sources I_1 and I_2 appearing in beams 1 and 2, $\underline{\underline{R}}'$ takes the form, using (40) and (31),

$$\underline{\underline{R}}' = \begin{bmatrix} \sqrt{\frac{I_1}{N} + 1} & & & 0 \\ & \sqrt{\frac{I_2}{N} + 1} & & \\ & & 1 & \\ & & & \ddots \\ 0 & & & 1 \end{bmatrix} \tag{41}$$

Assuming $I_1/N >> 1$ and $I_2/N >> 1$, the eigenvalue spread for $\underline{\underline{R}}'$ is given by $s'_1/s'_2 = \sqrt{I_1/I_2}$. Hence the compression parameter C defined in Eq. (31) is given by

$$C = \frac{10\log_{10}(I_1/I_2) - 10\log_{10}(I_1/I_2)^2}{10\log_{10}(I_1/I_2)} = .5 \tag{42}$$

Hence the maximum compression available from an ideal set of disjoint multiple beams using the hard-limiter modification is 50%, as contrasted to the theoretical limit of 100% for the pre-weighting scheme.

Consider now the example scenario treated previously and illustrated in Fig. 3. The corresponding eigenvalue spread for this case using the hard-limiter modification is listed in Table 3, assuming a 3% bandwidth. 34.8% compression relative to the conventional LMS algorithm is obtained. The time adaption of I_1/N and I_2/N is illustrated in Fig. 30, and the corresponding adapted contour at 1.33 msec. in Fig. 31. The "null" formed on the weaker interfering source is -13.3 dB, and -46.2 dB on the stronger source. These results can be compared to Figs. 4 and 5 obtained using the conventional LMS adaption and to Figs. 28 and 29 using the pre-weighting algorithm. The adapted radiation patterns for pre-weighting and hard-limiting are similar in form, suggesting that both techniques accomplish essentially the same result.

The average eigenvalue compression obtained by averaging over 10 randomly chosen scenarios was also computed using the hard-limiter modification applied to Cases 1 and 2 defined in Table 4. The results are tabulated in Tables 9 (Case 1, FBW = 0 and .0286) and 10 (Case 2, FBW = 0). The basic trends are similar to those using the pre-weighting scheme, with the degree of compression generally increasing as the number of beams increases.

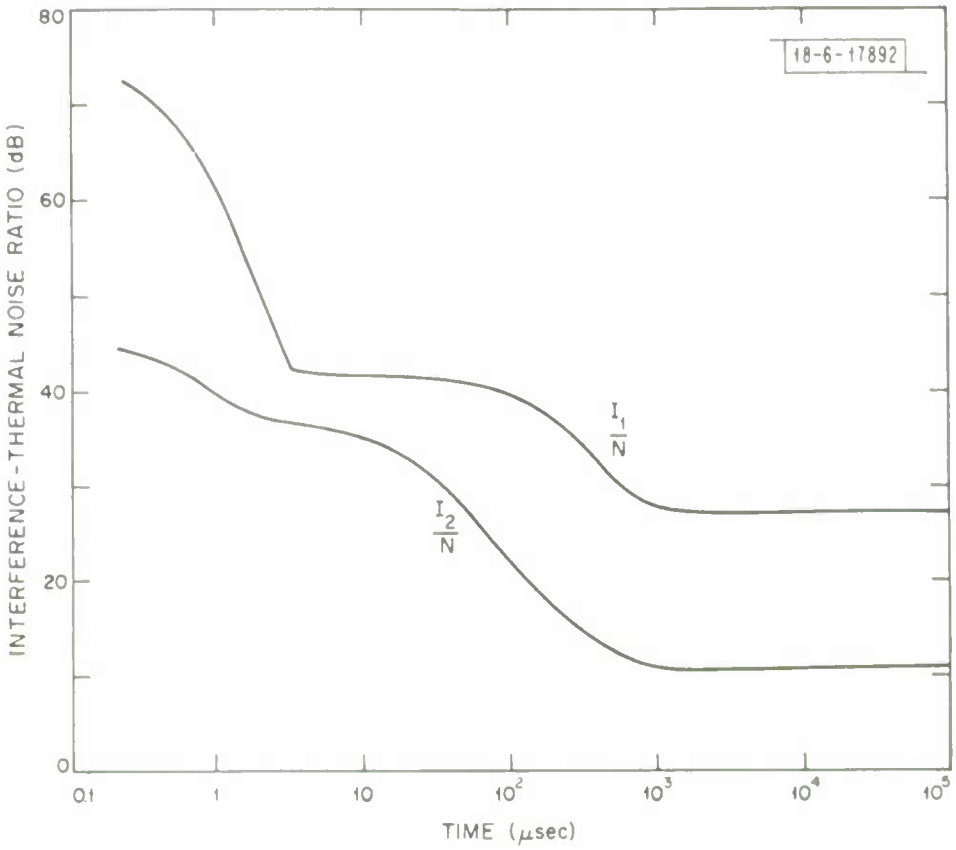

Fig. 30. Interference-thermal noise ratio vs time using hard-limiter in element feedback loop. Two-source interference scenario of Table 2. FBW = .0286.

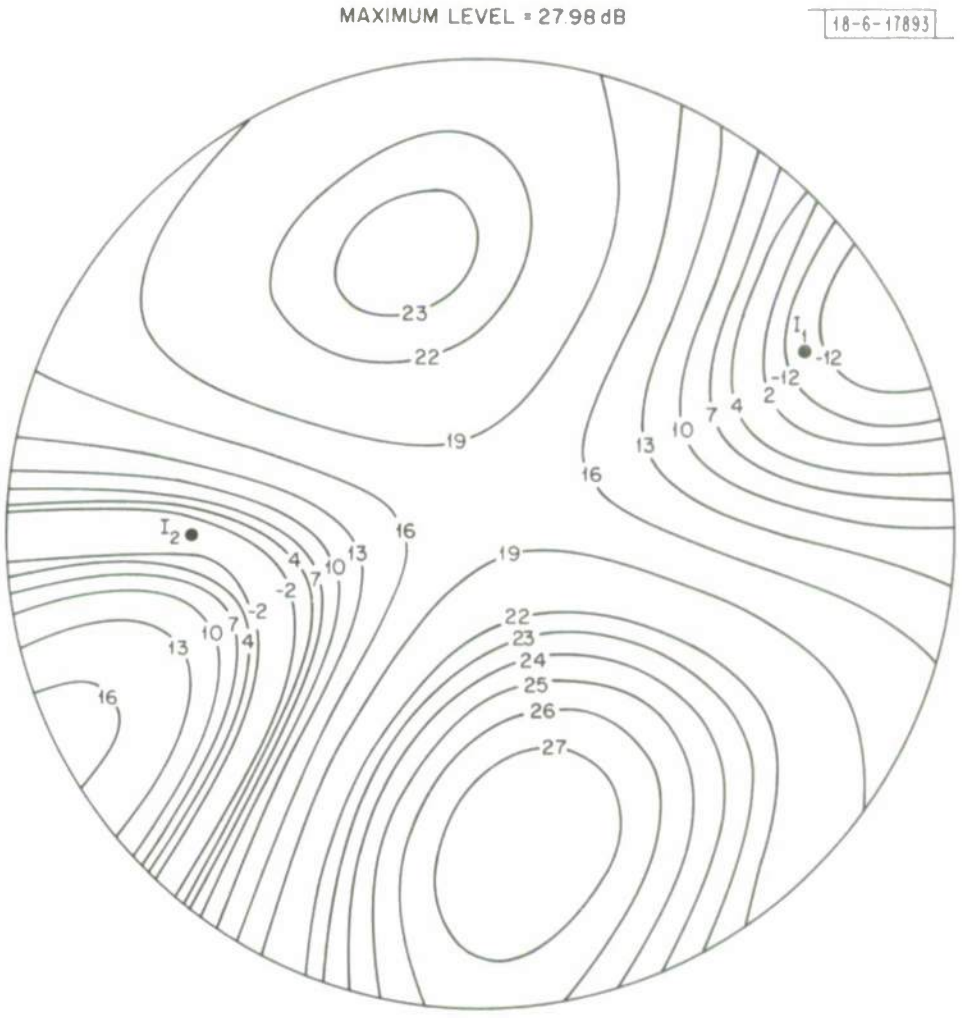

Fig. 31. Adapted radiation pattern using hard-limiter modification. Two-source scenario of Table 2.

Table 9

Eigenvalue Compression Using Hard-Limiter--Case 1.
FBW = 0, and FBW = .0286.

Case 1--FBW = 0

No. of Beams	Hard-Limiter	$(s_{MAX})_{AV}$	$(s_1/s_J)_{AV}$	Compression (%)
7	without	84.2 dB	48.3 dB	0
	with	86.4	40.3	16.7
19	without	88.4	34.3	0
	with	92.3	28.9	15.7
37	without	91.8	32.1	0
	with	96.4	25.0	22.1
61	without	94.2	31.6	0
	with	98.6	24.0	24.2

Case 1--FBW = .0286

No. of Beams	Hard-Limiter	$(s_{MAX})_{AV}$	$(s_1/s_{J+1})_{AV}$	Compression (%)
7	without	84.2	51.3	0
	with	86.4	42.9	16.4
19	without	88.4	38.5	0
	with	92.3	31.5	18.2
37*	without	91.6	35.2	0
	with	96.3	26.1	25.6

*Eight Cumulative Averages

Table 10

Eigenvalue Compression for Hard-Limiter--Case 2.
FBW = 0.

No. of Beams	Hard-Limiter	$(s_{MAX})_{AV}$	(s_1/s_J)	Compression C (Present)
7	without	84.2	32.4	----
	with	86.6	22.2	31.6
19	without	88.5	30.4	----
	with	92.1	22.1	27.3
37	without	91.7	30.5	----
	with	97.0	22.4	25.8
61	without	94.2	30.4	----
	with	99.1	20.3	33.2

VI. Discussion and Conclusions

Some of the more prominent features of a conventional LMS adaptive nulling algorithm when used in conjunction with a multiple-beam antenna have been presented. When contrasted to a linear or planar array, it has been shown that the MBA has several features which tend to enhance the versatility of the conventional algorithm. First, and foremost, the MBA offers power discrimination from beam port to beam port, which can be used to enhance the dynamic range of interference power levels which the algorithm can sense and null. This is accomplished either by pre-weighting at the beam port before adaption begins, or hard-limiting in the element feedback loop. Secondly, as the aperture size and number of beams increases, the power discrimination between beam ports tends to "decouple" the adaptive loops (i.e., only those loops having beams in the vicinity of the interfering sources are significantly modified), suggesting that constraints on allowable error tolerances between loops might be able to be relaxed somewhat. Finally, use of an MBA with a set of beams fixed in position should lead to a more broadband frequency sensitivity.

Three techniques for accomplishing eigenvalue compression, particularly suitable to multiple-beam antennas, have been discussed. Using the pre-weighting technique, one first samples the output power of each beam port, and inserts pre-weighting into those ports where large interference sources are present in order to obtain some pattern shaping on the larger sources before adaption begins. The quiescent loop gain can then be adjusted so that the full dynamic range of the adaptive processing is made available to the weaker interfering sources. Depending on the number of beams, and the

number of interference sources anywhere from 25-50% average compression can be obtained, relative to no pre-weighting for a fixed number of beams. Increasing the number of beams (with the corresponding increase in aperture diameter) leads to a further reduction in eigenvalue spread. Using a hard-limiter in the element feedback loop leads to similar results but the compression is somewhat less than when using pre-weighting. Use of these compression techniques allows for a significant enhancement in the allowable dynamic range of interfernece power levels which the algorithm can handle. Alternately, one can use the compression obtained in order to decrease the adaption time, or decrease the nulling bandwidth for a fixed dynamic range.

We have also examined the possibility of combining hard-limiting and pre-weighting. The results for the Case 1, six source scenarios are tabulated in Table 11. Comparing these results with those in Tables 5 and 6, using pre-weighting only, indicates that combining the compression techniques does not significantly enhance the compression. We conclude that pre-weighting alone offers the best technique for compression the eigenvalues, and including a hard-limiter in the element branch feedback loop in order to enhance the dynamic range of control-loop feedback voltages slightly enhances the compression obtained by pre-weighting.

Table 11

Eigenvalue Compression Using Hard-Limiter and 30 dB Pre-Weighting--
Case 1 - FBW = 0.

Case 1--FBW = 0

No. of Beams	Hard-Limiter	$(s_{MAX})_{AV}$	$(s_1/s_J)_{AV}$	% dB Compression
7	without	84.2	48.3	----
	with	69.1	36.6	24.2 %
19	without	88.4	34.3	----
	with	75.6	26.7	22.1 %
37	without	91.6	32.3	----
	with	79.7	21.9	32.0 %
61	without	94.2	31.6	----
	with	81.9	21.7	31.3 %

Case 1--FBW = .0286

No. of Beams	Hard-Limiter	$(s_{MAX})_{AV}$	(s_1/s_{J+1})	% dB Compression
7	without	84.2	51.3	----
	with	69.1	39.6	22.8 %
19	without	88.4	38.5	----
	with	75.6	28.1	27.0 %
37	without	91.6	35.2	----
	with	79.6	22.8	36.2 %

APPENDIX A

In this appendix we consider minimizing the total received interference-thermal noise ratio at the output of the array, subject to the fixed constraint that the adapted weights $\underline{w}$ approximate the desired weights as closely as possible as possible. Thus we desire to obtain solutions to the minimization problem

$$\underset{\underline{w}}{\text{MIN}}\{I/N\} = \underset{\underline{w}}{\text{MIN}} \frac{\underline{w}^{\dagger} \cdot \underline{\underline{M}}_I \cdot \underline{w}}{\underline{w}^{\dagger} \cdot \underline{\underline{M}}_N \cdot \underline{w}} \tag{A1}$$

subject to the fixed constraint

$$|\underline{w} - \underline{w}_o|^2 = \varepsilon \tag{A2}$$

where ε is an arbitrary constant. The set of weights $\underline{w}$ satisfying (A1) and (A2) is a strong function of ε. Intuitively we anticipate that if we choose ε very small, then we essentially require $\underline{w} = \underline{w}_o$ and the radiation pattern evaluated in the direction of the interference does not change. However, as ε increases, solutions to (A1) and (A2) gradually result in reducing the directivity in the direction of the interfering source; finally, by further increasing ε, a critical value is reached when the total output power I/N is reduced to zero, and the remaining degrees of freedom are used to best approximate $\underline{w}$ to $\underline{w}_o$. We note that the role played by the parameter ε is precisely that of the parameter μ_o in the Applebaum-Howell control loop. As $\mu_o \to 0$ (i.e., either small loop gain or large effective thermal noise), the loop does not sense the interfering source and the steady state weights adapt

so that $\underline{w} \simeq \underline{w}_o$. As μ_o increases, the loops begin to sense the larger sources, and adapt so as to place minima (but not nulls) in the direction of these sources. If we would increase $\mu_o >> 1$ (very large gain in the loops) then the adapted weights would essentially place nulls on all the received signals, assuming the degrees of freedom are not all used up.

In order to illustrate this correspondence more clearly, consider the variational solution to (A1) and (A2). We form the variational function

$$F\{\underline{w}\} = \underline{w}^{\dagger} \cdot \underline{\underline{M}}_I \cdot \underline{w} + \lambda_1 \underline{w}^{\dagger} \cdot \underline{\underline{M}}_N \cdot \underline{w} + \lambda_2 |\underline{w} - \underline{w}_o|^2 \tag{A3}$$

The minimization criteria is given by $\nabla_{\underline{\omega}} F = 0$. We obtain

$$[\underline{\underline{M}}_I + \lambda_1 \underline{\underline{M}}_N + \lambda_2 \underline{\underline{I}}] \cdot \underline{w} = \lambda_2 \underline{w}_o \tag{A4}$$

Solving for $\underline{w}$:

$$\underline{w} = [\underline{\underline{I}} + \frac{1}{\lambda_2} (\underline{\underline{M}}_I + \frac{\lambda_1}{\lambda_2} \underline{\underline{M}}_N)]^{-1} \cdot \underline{w}_o \tag{A5}$$

In comparing Eq. (A5) to Eq. (16), we observe the correspondence $\frac{1}{\lambda_2} \leftrightarrow \mu_o$. Clearly $\lambda_2 \to 0$ corresponds to $\mu_o >> 1$, in which case the solution to (A4) place perfect nulls on the interference irrespective of the desired weights $\underline{w}_o$. For $\lambda_2 >> 1$ and $I >> N$, which is the primary case of interest,

$$\underline{w} \simeq [\underline{\underline{I}} + \frac{1}{\lambda_2} \underline{\underline{M}}_I]^{-1} \cdot \underline{w}_o \tag{A6}$$

which agrees with the steady state solution, Eq. (19), obtained for the Applebaum loop. In order to precisely evaluate λ_2 in terms of the constraint parameter ε, one should substitute (A6) into (A2) and solve for λ_2. The

result is complicated and it is not felt to be of prime importance to carry out the calculation.

Finally we note the relation to the constraint (A2) to radiation pattern shaping. The rms pattern error can be expressed in terms of the excitation currents on the feed elements in the form

$$\Delta\varepsilon = (\underline{I} - \underline{I}_o)^{\dagger} \cdot \underline{\underline{B}} \cdot (\underline{I} - \underline{I}_o) \tag{A7}$$

where $\underline{I}$ is the excitation current, $\underline{I}_o$ the desired excitation current and $\underline{\underline{B}}$ the beam coupling matrix. When $\underline{\underline{B}}$ is normalized to unity maximum diagonal element we have $\underline{\underline{B}} = \underline{\underline{R}}_N$. The excitation currents $\underline{I}$ on the feed elements are related to the weights $\underline{w}$ according to the results of Appendix B:

$$\underline{I} = [\underline{\underline{I}} + \underline{\underline{R}}_n]^{-1} \cdot \underline{w} \tag{A8}$$

Using (A8) in (A7), we obtain

$$\Delta\varepsilon = (\underline{w}-\underline{w}_o)^{\dagger} \cdot [\underline{\underline{I}} + \underline{\underline{R}}_N]^{-1} \cdot \underline{\underline{R}}_N \cdot [\underline{\underline{I}} + \underline{\underline{R}}_N]^{-1} \cdot (\underline{w}-\underline{w}_o) \tag{A9}$$

Since the off-diagonal elements of $\underline{\underline{R}}_N$ correspond to the mutual coupling between elements, which is generally less than, say 10 dB, the matrix $\underline{\underline{I}} + \underline{\underline{R}}_N$ is nearly diagonal. Thus the matrix $[\underline{\underline{I}} + \underline{\underline{R}}_N]^{-1} \cdot \underline{\underline{R}}_N \cdot [\underline{\underline{I}} + \underline{\underline{R}}_N]^{-1}$ is even more nearly diagonal. Indeed, for the ideal beams we used considered to model the MBA, the off diagonal terms are essentially two orders of magnitude down from the diagonal terms. Thus (A9) is a very good approximation to the rms weight constraint (A2), and rms pattern synthesis is essentially equivalent to rms approximation to the desired weight. This has also been demonstrated via simulations comparing the two techniques.

APPENDIX B

In this appendix we derive Eq. (9) specifying the correlation matrix at the receive beam ports including the effects of mutual coupling. Consider, for example, the K-element feed network and reflector antenna structure illustrated in Fig. B1a. On reception, the voltages and currents induced at terminals of the feed cluster (denoted x-x) are fed into a K-port load $\underline{\underline{Z}}_L$ representing the receive circuitry of the array. For purposes of analysis, the multi-terminal network at terminals x-x can be modeled by its K-port Thevenin equivalent circuit, illustrated in Fig. B1b. The voltage generators $V_{01},\cdots,V_{0K}$ represent the "open circuit" voltages induced at terminals x-x when no load is attached. In vector form, we define

$$\underline{V}_0 = \begin{bmatrix} V_{01} \\ V_{02} \\ \cdot \\ \cdot \\ \cdot \\ V_{0K} \end{bmatrix} \tag{B1}$$

The voltages V_{0K} are functions of the electric field <u>incident</u> on the array. $\underline{V}_0$ will be evaluated later. The impedance matrix $\underline{\underline{Z}}$ represents the input impedance looking into the terminals x-x when $\underline{V}_0 = 0$, i.e., when the array is transmitting. Thus the matrix $\underline{\underline{Z}}$ includes the self- and mutual-coupling of complete reflector plus feed cluster. If we define the voltage $\underline{V}$ and currents $\underline{I}$ at the terminals x-x as shown in Fig. B1b (note, the current convention for $\underline{I}$ is taken flowing out of x-x), then the $\underline{V}$ and $\underline{I}$ are related according to [8]

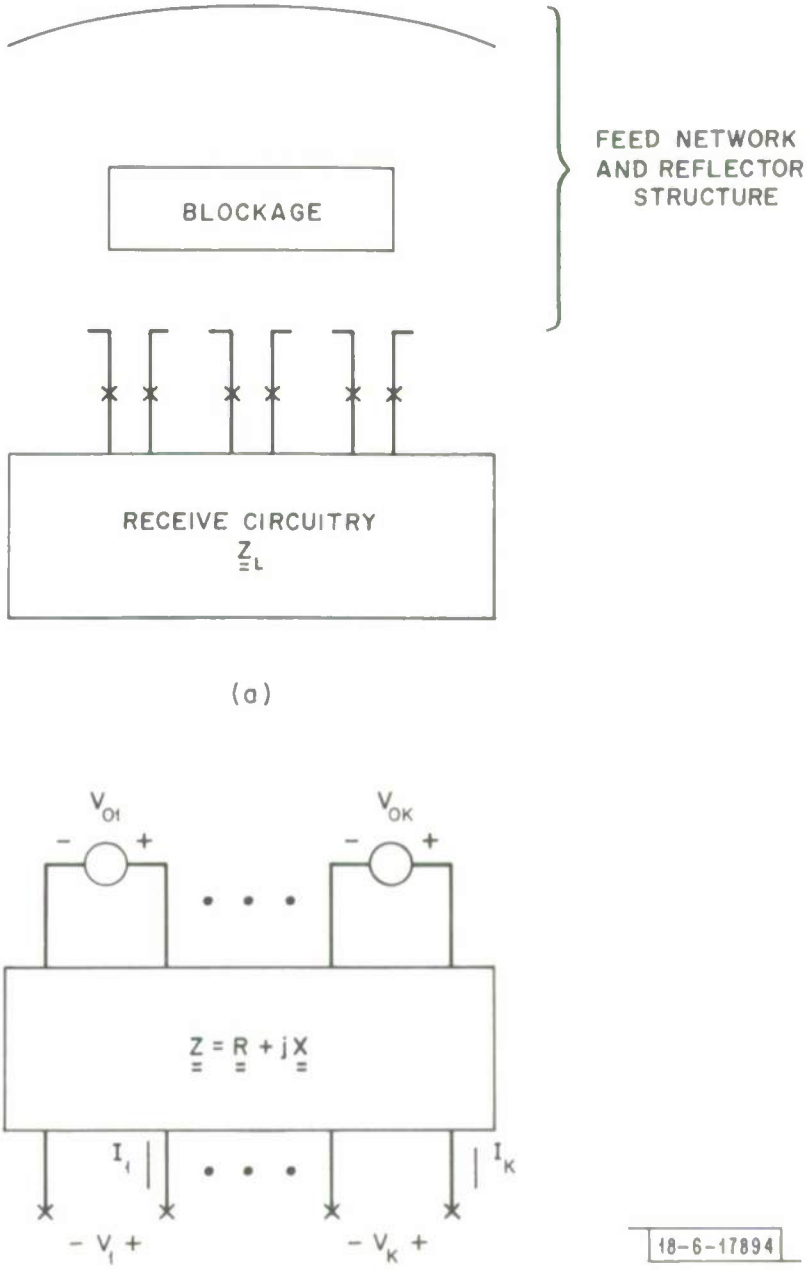

Fig. B1. a. Feed network and reflector struction for a multiple-beam antenna. b. K-port equivalent circuit of Fig. B-1 a.

$$\underline{V} = \underline{V}_0 - \underline{\underline{Z}} \cdot \underline{I} \tag{B2}$$

Ideally one desires to attach a load network $\underline{\underline{Z}}_L$ to x-x as shown in Fig. B1a so as to extract maximum power from the incident wavefront. This optimum load can readily be shown to be[9] $\underline{\underline{Z}}_L = \underline{\underline{Z}}^*$, where the * denotes complex conjugate. This optimum load is necessarily a K-port coupled network. From a practical viewpoint, since we desire to process the received signal through a summing network to a single port, it is generally difficult to achieve the optimum matching $\underline{\underline{Z}}_L = \underline{\underline{Z}}^*$. Rather, one usually resorts to the non-optimum matching network illustrated in Fig. B2. Defining $\underline{\underline{Z}} = \underline{\underline{R}} + j\underline{\underline{X}}$, we insert a reactive matching network $-j\underline{\underline{X}}$ fed by K transmission lines of characteristic impedance R_o. Realization of the receive matching network has been developed by Block[8] and is illustrated in Fig. B3. The reactive cancellation is accomplished by introducing reactive cross-coupling $-jX_{kq}$ between each kth and qth ports, and inserting a series cancellation $-jX_{kk}$ at the kth port and $-jX_{qq}$ at the qth port. The characteristic impedance R_o in each line assumes a matched impedance R_o looking into the sum network from each feed line. The weights $w_1,\cdots,w_k$ inserted in the feed lines R_o are assumed matched to R_o. Thus for this load, the K-port load impedance as seen from the terminals x-x is given by

$$\underline{\underline{Z}}_L = R_o\underline{\underline{I}} - j\underline{\underline{X}} \tag{B3}$$

where $\underline{\underline{I}}$ denotes the identy matrix. Using Eqs. (B3) and (B2), and noting that at x-x, $\underline{V} = \underline{\underline{Z}}_L \cdot \underline{I}$, we can solve for the current $\underline{I}$ flowing out of the terminals x-x and into the transmission line R_o. We obtain

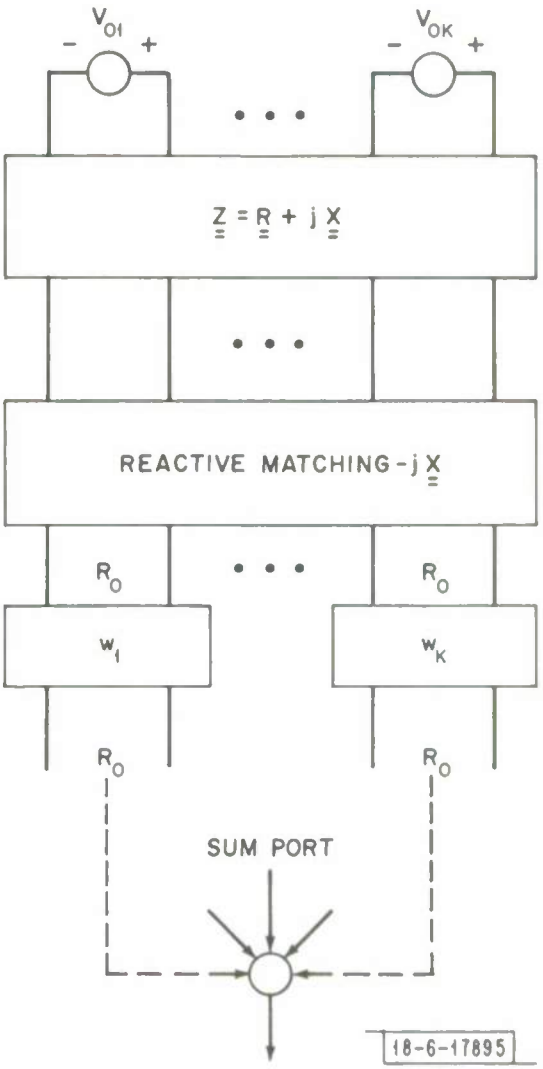

Fig. B2. Reactively matched transmission line feed network employing a single receive port.

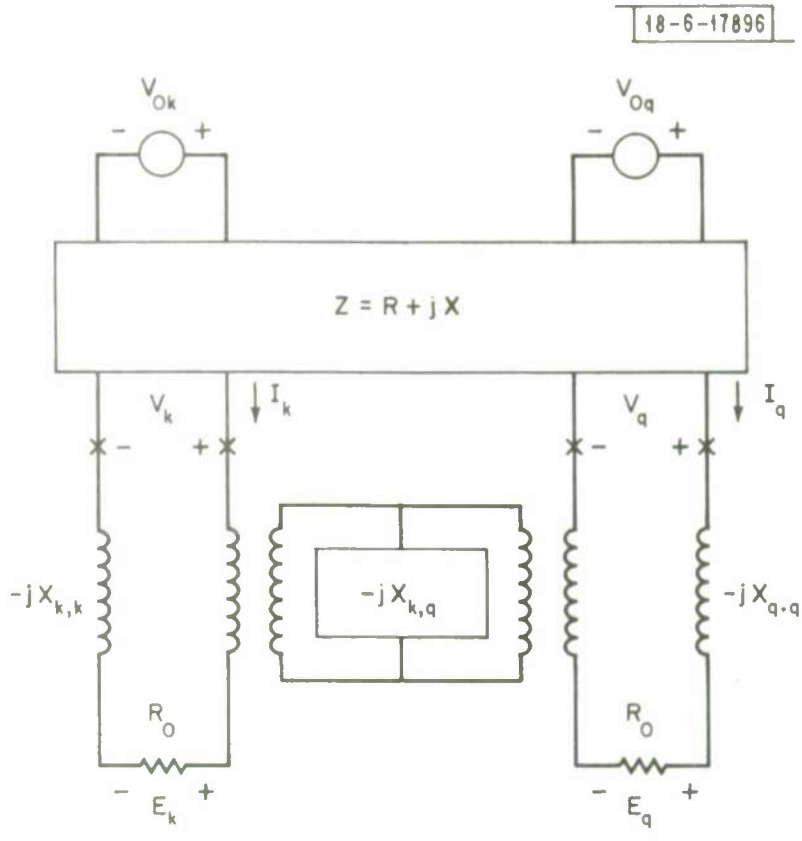

Fig. B3. Physical realization of reactive matching network of Fig. B2 between ports k and q.

$$\underline{I} = [\underline{\underline{R}} + R_o \underline{\underline{I}}]^{-1} \cdot \underline{V}_o \tag{B4}$$

Define the voltage $\underline{E}$ across the transmission line R_o. Then $\underline{E} = R_o \underline{I}$, and we obtain

$$\underline{E} = [\underline{\underline{I}} + \underline{\underline{R}}/R_o]^{-1} \cdot \underline{V}_0 \tag{B5}$$

It is convenient to define the normalized resistive matrix $\underline{\underline{R}}_N$

$$\underline{\underline{R}}_N \equiv \frac{1}{R_o} \underline{\underline{R}} \tag{B6}$$

in which case we obtain

$$\underline{E} = [\underline{\underline{I}} + \underline{\underline{R}}_N]^{-1} \cdot \underline{V}_0 \tag{B7}$$

The voltages $E_1, \cdots, E_K$ are, respectively, weighted by the weights $w_1, \cdots, w_K$, and the average power received at the sum port is given by

$$P_{Rec} = \frac{1}{R_o} \overline{|\underline{w}^\dagger \cdot \underline{E}|^2} = \frac{1}{R_o} \underline{w}^\dagger \cdot \overline{\underline{E}\underline{E}^\dagger} \cdot \underline{w} \tag{B8}$$

where $\underline{w}$ is a column vector of the weights, and "†" denotes "complex-conjugate transpose". We define the super bar notation to denote the average over frequency, ω, according to

$$\overline{(\cdot)} = \frac{1}{BW} \int_{\omega_o - \frac{BW}{2}}^{\omega_o + BW/2} (\cdot)\, d\omega$$

where BW is the receiver bandwidth centered about $\omega = \omega_o$. We note that the total average power delivered to the receive network is given by

$$P_{R_o} = \frac{1}{R_o} \overline{\underline{E}^\dagger \cdot \underline{E}} \tag{B9}$$

The average power dissipated in the weights $\underline{w}$ is given by

$$P_{\underline{\omega}} = \frac{1}{R_o} \sum_{k=1}^{K} \overline{|\omega_k E_k|^2} \tag{B10}$$

Hence the average power dissipated in the summing network, P_Σ, must be

$$P_\Sigma = \frac{1}{R_o} \overline{\underline{E}^\dagger \cdot \underline{E}} - \frac{1}{R_o} \overline{|\underline{w}^\dagger \cdot \underline{E}|^2} - \frac{1}{R_o} \sum_{k=1}^{K} \overline{|w_k E_k|^2} \tag{B11}$$

The correlation matrix $\overline{\underline{\underline{M}}}$ arising from signals incident on the array, as measured at the input to the feed line R_o, is defined according to the average received power. We define $\overline{\underline{\underline{M}}}$ according to

$$P_{Rec} = \underline{w}^\dagger \cdot \overline{\underline{\underline{M}}} \cdot \underline{w} \tag{B12}$$

Comparing Eqs. (B12) and (B8), we obtain

$$\overline{\underline{\underline{M}}} = \frac{1}{R_o} \underline{E}\, \underline{E}^\dagger \tag{B13}$$

If J incoherent signals are incident on the antenna, then we have

$$\overline{\underline{\underline{M}}} = \frac{1}{R_o} \sum_{j=1}^{J} \overline{E_j E_j^\dagger} \tag{B14}$$

where $\underline{E}_j$ is defined as in (7) for each $j = 1, \cdots, J$. If J <u>coherent</u> signals are incident on the antenna we have

$$\overline{\underline{\underline{M}}} = \frac{1}{R_o} \overline{\left(\sum_{j=1}^{J} E_j \right) \left(\sum_{j=1}^{J} \underline{E}_j \right)^\dagger} \tag{B15}$$

The effect on $\underline{\underline{M}}$ of adding either internal thermal noise or external omi-directional noise will be considered in a later section. It still remains to evaluate the induced voltages $V_{01},\cdots,V_{0K}$ in terms of the signals incident on the antenna structure.

A. Evaluation of $\underline{V}_0$

Since the voltages $\underline{V}_0$ depend only on the amplitude and phase of the incident electric field, and not on the matching condition, we can determine each V_{0k} by considering the power dissipated in each isolated port under matched conditions, and apply reciprocity. To see this, consider the Thevenin voltage-current relationship at the terminals x-x as defined by Eq. (B2). We first evaluate V_{01}. If we open circuit ports $2,3,\cdots,K$, then $I_2 = \cdots = I_K = 0$ and Eq. (2) reduces to

$$V_1 = V_{01} - Z_{11}I_1 \tag{B16}$$

We now attach a load Z_{11}^* to port 1 as illustrated in Fig. B4. Thus $V_1 = Z_{11}^* I_1$ and we obtain

$$I_1 = V_{01}/2R_{11} \tag{B17}$$

The power dissipated in the load resistor R_{11} is then given by

$$P_1 = R_{11}|I_1|^2 = \frac{|V_{01}|^2}{4R_{11}} \tag{b18}$$

We now apply the reciprocity concept to evaluate V_{01} in terms of the incident field. Consider an incident power flux $P_J G_J/4\pi R^2$, where $P_J G_J$ denotes the ERP transmitted from a source located at the position (θ_J,ϕ_J). Since port 1

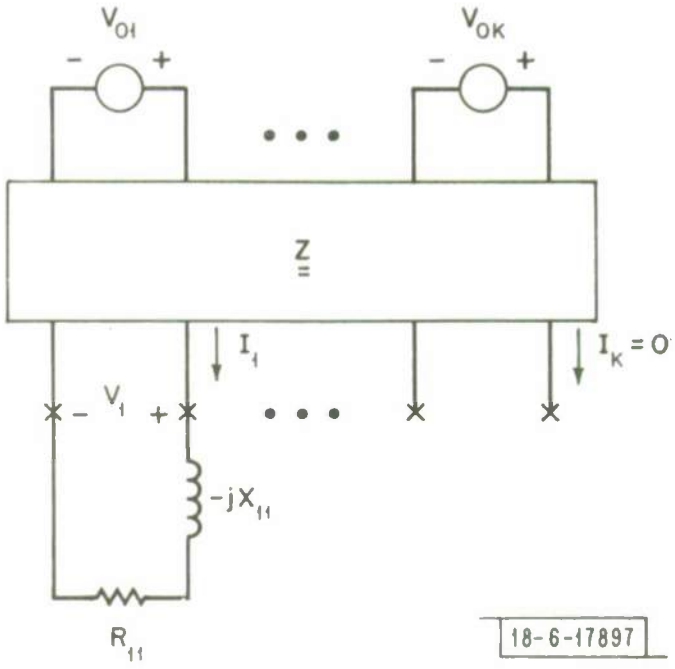

Fig. B4. Port 1 terminated in matched load Z_{11}^*. Ports 2, 3,$\cdots$,K open circuited.

is matched, the received power must be given by

$$P_1 = \frac{P_J G_J}{4\pi R^2} (A_e)_1 \tag{B19}$$

where A_{e_1} denotes the effective area of port 1 with port 2,$\cdots$K open circuited. By reciprocity, and since the load Z_{11}^* is matched for maximum power absorption, then $(A_e)_1 = \lambda^2 D_1/4\pi$, where D_1 is the directivity of the multiple-beam antenna (MBA) excited at port 1 (other ports open circuited). Comparing (B19) and (B18) we obtain

$$|V_{01}|^2 = 4R_{11} P_J G_J \left(\frac{\lambda}{4\pi R}\right)^2 D_1(\theta_J,\phi_J) \tag{B20}$$

The phase of V_{01} must be that of the incident field seen at port 1 relative to some fixed reference point. Denoting this phase by ψ_1, we have

$$V_{01} = 2\sqrt{R_{11} P_J G_J}\left(\frac{\lambda}{4\pi R}\right)\sqrt{D_1(\theta_J,\phi_J)}\, e^{j\psi_1}$$

Generalizing this result to each of the K receive ports, we have

$$\underline{V}_0 = 2\sqrt{P_J G_J}\left(\frac{\lambda}{4\pi R}\right)\begin{bmatrix} \sqrt{R_{11} D_1(\theta_J,\phi_J)}\, e^{j\psi_1} \\ \sqrt{R_{22} D_2(\theta_J,\phi_J)}\, e^{j\psi_2} \\ \vdots \\ \sqrt{R_{KK} D_K(\theta_J,\phi_J)}\, e^{j\psi_K} \end{bmatrix} \tag{B22}$$

Using (B22), (B7) and either (B14) or (B15) then leads to the proper expression for the correlation matrix $\underline{\underline{M}}$ in terms of the signals incident on the MBA.

It is useful to examine the correlation matrix $\underline{\underline{M}}$ under the assumption of idealized maximum directivity beams considered previously.[3] In this case, we have[†]

$$D_k(\theta_J,\phi_J) = \left(\frac{4\pi A}{\lambda^2}\right) \phi_k(\theta_J,\phi_J) \qquad k=1,\cdots,K \tag{B23}$$

where the set of normalized beams $\{\phi_k\}$, correspond to shifted $J_1(x)/x$ beams radiated from the multiple beam antenna. For this set of beams, one can show that $R_{11} \approx R_{22} \approx \cdots \approx R_{KK}$ and $\psi_1 = \cdots = \psi_K = 0$. Thus a convenient choice for R_o is then $R_o = R_{11}$. With these assumptions the correlation matrix $\underline{\underline{\bar{M}}}$ takes the form

$$\underline{\underline{\bar{M}}} = P_J G_J \left(\frac{\lambda}{4\pi R}\right)^2 \frac{4\pi A}{\lambda^2} \overline{4[\underline{\underline{I}} + \underline{\underline{R}}_N]^{-1} \cdot \underline{c}\,\underline{c}^{\dagger} \cdot [\underline{\underline{I}} + \underline{\underline{R}}_N]^{-1}} \tag{B24}$$

where we define

$$\underline{c} \equiv \begin{bmatrix} \phi_1(\theta_J,\phi_J) \\ \phi_2(\theta_J,\phi_J) \\ \vdots \\ \phi_k(\theta_J,\phi_J) \end{bmatrix} \tag{B25}$$

B. Effects of Internal and External Noise

In the presence of either internal or external noise, the correlation matrix must be appropriately modified. If internal, uncorrelated white noise is inserted at the inputs to each beam port, then the resultant noise power at the output, assuming equal noise power, N, in each channel, is given by

[†] A is the physical area of the reflector.

$$(P_o)_i = \underline{w}^\dagger \cdot N \underline{\underline{I}} \cdot \underline{w}^\dagger \tag{B26}$$

For external, omni-directional noise we define the incident noise flux/unit solid angle as $P_e = P_N/4\pi$. Using (B24), the total received noise power from all directions is then given by

$$(P_o)_e = \frac{P_N}{4\pi}\ \underline{w}^\dagger \cdot 4\left(\frac{1}{BW}\right) \int_{\omega_o - \frac{BW}{2}}^{\omega_o + \frac{BW}{2}} d\omega \left\{ [\underline{\underline{R}}_N + \underline{\underline{I}}]^{-1} \cdot \int_{\text{all space}} \underline{c}\,\underline{c}^\dagger\, d\Omega \cdot [\underline{\underline{R}}_N + \underline{\underline{I}}]^{-1} \right\} \cdot \underline{w} \tag{B27}$$

where $d\Omega$ is the differential solid angle $d\Omega = \sin\theta d\theta d\phi$, and $d\omega$ is the differential frequency. If we define the beam coupling matrix $\underline{\underline{B}}$ according to

$$\underline{\underline{B}} \equiv \frac{1}{4\pi}\ \left(\frac{4\pi A}{\lambda^2}\right) \int_{\text{all space}} \underline{c}\,\underline{c}^\dagger\, d\Omega \tag{B28}$$

we obtain

$$(P_o)_e = P_N\, \underline{w}^\dagger \cdot 4\left(\frac{1}{BW}\right) \int_{\omega_o - \frac{BW}{2}}^{\omega_o + \frac{BW}{2}} \left\{ [\underline{\underline{R}}_N + \underline{\underline{I}}]^{-1} \cdot \underline{\underline{B}} \cdot [\underline{\underline{R}}_N + \underline{\underline{I}}]^{-1} d\omega \right\} \cdot \underline{w} \tag{B29}$$

Assuming $\underline{\underline{B}}$ and $\underline{\underline{R}}_N$ are only slowly varying functions of frequency, we approximate

$$(P_o)_e \approx P_N\, \underline{w}^\dagger \cdot 4[\underline{\underline{R}}_N + \underline{\underline{I}}]^{-1} \cdot \underline{\underline{B}} \cdot [\underline{\underline{R}}_N + \underline{\underline{I}}]^{-1} \cdot \underline{w} \tag{B30}$$

Combining (B26) and (B30) and (B24) we obtain the total correlation matrix for the MBA upon reception for the unmatched received circuit illustrated in

Fig. B2:

$$\underline{\underline{M}} = P_J G_J \left(\frac{\lambda}{4\pi R}\right)^2 \left(\frac{4\pi A}{\lambda^2}\right) 4[\underline{\underline{I}} + \underline{\underline{R}}_N^{-1}] \cdot \overline{\underline{c}\,\underline{c}^{\dagger}} \cdot [\underline{\underline{I}} + \underline{\underline{R}}_N]^{-1}$$

$$+ N \underline{\underline{I}} + P_N 4[\underline{\underline{R}}_N + \underline{\underline{I}}]^{-1} \cdot \underline{\underline{B}} \cdot [\underline{\underline{R}}_N + \underline{\underline{I}}]^{-1} \qquad \text{(B31)}$$

Noting from network theory, assuming a lossless load, the radiated power on transmission must be proportional to $\underline{I}^{\dagger} \cdot \underline{\underline{R}}_N \cdot \underline{I}$. Using field theory, we also obtain from Poynting's theorem that the radiated power is proportional to $\underline{I}^{\dagger} \cdot \underline{\underline{B}} \cdot \underline{I}$. Hence we can take $\underline{\underline{R}}_N$ = Normalized $\underline{\underline{B}}$ of Eq. (B28). Dividing through by N leads to the normalized $\underline{\underline{R}}$ given by Eq. (9) of the text.

References

1. W. F. Gabriel, Proc. IEEE 64, 239-271 (1976).

2. L. E. Brennan, E. L. Pugh, and I. S. Reed, IEEE Trans. Aerospace Electron. System AES-7, 254-262 (1971).

3. J. T. Mayhan, "Nulling Limitations for a Multiple-Beam Antenna," IEEE Trans. Antennas Propag. (To be published.)

4. J. Ruze, IEEE Trans. Antennas Propag. AP-13, 660 (1965), Fig. 7, DDC AD-625018.

5. J. T. Mayhan and L. J. Ricardi, IEEE Trans. Antennas Propag. AP-23, 639 (1975), DDC AD-A017357/5.

6. L. J. Ricardi, A. J. Simmons, A. R. Dion, L. K. DeSize, and B. M. Potts, "Some Characteristics of a Communication Satellite Multiple-Beam Antenna," Technical Note 1975-3, Lincoln Laboratory, M.I.T. (28 January 1975), DDC AD-A006405/5.

7. L. E. Brennan and I. S. Reed, IEEE Trans. Aerospace Electron. Systems AES-7, 698 (1971).

8. A. Block, Wireless Engineering, (December 1956).

9. R. F. Harrington, Field Computation by Moment Methods (McGraw-Hill, New York, 1968).

OUTSIDE DISTRIBUTION LIST

Aerospace Corp.
Bldg. 110, Rm. 1364
2350 East El Segundo Blvd.
El Segundo, CA 90245

C. Bredall
C. Colburn
F. L. Hennessey
E. G. Todd

Defense Communications Agency
8th and South Courthouse Road
Arlington, Virginia

Dr. F. E. Bond, Code 800
Capt. David Fischer
Col. S. Shaffran
R. Drummond

Defense Communications Eng. Center
1860 Wiehle Avenue
R-405
Reston, Virginia 22090

N. Brienza
R. Donovan
T. Ellington

Dr. James Babcock
Staff Specialist for Satellites
(Development & Acquisition)
ODTACCS, Rm. 3D161
Pentagon
Washington, D. C. 20301

Mr. Donald K. Dement, ECE
NASA Headquarters
600 Independence Ave., S.W.
Washington, DC 20546

Capt. J. Pope
NESC PME-106
Naval Electronics System Command
Washington, D. C.

Lt. Cmdr. C. J. Waylan
NESC PME-106
Naval Electronics System Command
Washington, D. C.

J. DonCarlos, PME-117T
Dept. of the Navy
Washington, D.C.

Naval Research Laboratory
Attn: Mr. R. LaFonde
4555 Overlook Avenue, S.W.
Washington, D.C. 20390

Dr. W. Gabriel
Dr. F. Staudaher

RADC/ETE
A. C. Schell
Stop 30
Hanscom Air Force Base
Bedford, MA

RADC/DCCR
Griffiss AFB
Rome, New York 13441

Dr. F. Diamond
J. Graniero
T. Trendway

SAMSO
P. O. Box 92960
Worldway Postal Center
Los Angeles, CA 90009

Col. R. Miller
Capt. E. Nicastri
Col. H. Wynne
Lt. Col. D. Mills

Paul Forrest
TRI-TAC
Ft. Monmouth, N.J. 07703

R. G. Gould
Suite 521E
7315 Wisconsin Avenue
Washington, D.C. 20014

Joseph Lin
Syracuse University Research Center
Merrill Lane
University Heights
Syracuse, New York 13210

David Arnold
Airborne Instruments Laboratory
Deer Park
Long Island, New York 11729

W. Masenten
Hughes Aircraft Co.
Comm. & Radar Div.
1901 Malvern Street, P. O. Box 3310
Fullerton, CA 92634

Andrew Zeger
General Atronics
1200 East Mermaid Lane
Philadelphia, PA 19118

Dr. A. C. Vosberg
Dr. K. L. Jordan
SAFRD
Room 4D977, Pentagon
Washington, D.C. 20301

J. Dupree
TRW Systems Group
One Space Park
Redondo Beach, CA

Army

Lt. Col. J. D. Thompson
Attn: DAMO-TCS
Dept. of the Army
Washington, D.C. 20310

Mr. D. L. LaBanca
U.S. Army Satellite Communications Agency
Attn: AMCPM-SC511
Building 209
Fort Monmouth, N.J. 07703

Headquarters
Deptartment of the Army
Attn: DAMA-CSC
Washington, D.C. 20310

Navy

Dr. R. Conley
Office of Chief of Naval Operations
Attn: 094H
Deptartment of the Navy
Washington, D.C. 20350

Capt. R. E. Enright
Office of Chief of Naval Operations
Attn: 941E
Washington, D.C. 20350

Mr. D. McClure
Office of Naval Telecommunications System Architect
3801 Nebraska Avenue
Washington, D.C. 20390

Marine Corps

Major G. P. Criscuolo
Attn: CE
Headquarters, U.S. Marine Corps.
Washington, D. C. 20380

Air Force

Col. J. C. Mayers
Attn: RDSC
Headquarters, U.S. Air Force
Washington, D.C. 20330

Lt. Col. J. C. Wright
Attn: PRCXP
Headquarters, U.S. Air Force
Washington, D.C. 20330

JLC

Lt. Col. J. S. Tuck
Organization Joint Chiefs of Staff
Attn: J-6
Washington, D.C. 20301

Mr. S. L. Stauss
Organization Joint Chiefs of Staff
Attn: J-3
Washington, D.C. 20301

NSA

Mr. George Jelen, Jr.
National Security Agency
Attn: S-26
Ft. George G. Meade, MD 20755

Mr. David Bitzer
National Security Agency
Attn: R-12
Ft. George G. Meade, MD 20755

REPORT DOCUMENTATION PAGE		READ INSTRUCTIONS BEFORE COMPLETING FORM
1. REPORT NUMBER ESD-TR-76-304	2. GOVT ACCESSION NO.	3. RECIPIENT'S CATALOG NUMBER
4. TITLE (and Subtitle) Adaptive Nulling with Multiple-Beam Antennas		5. TYPE OF REPORT & PERIOD COVERED Technical Note 6. PERFORMING ORG. REPORT NUMBER Technical Note 1976-18
7. AUTHOR(s) Joseph T. Mayhan		8. CONTRACT OR GRANT NUMBER(s) F19628-76-C-0002
9. PERFORMING ORGANIZATION NAME AND ADDRESS Lincoln Laboratory, M.I.T. P.O. Box 73 Lexington, MA 02173		10. PROGRAM ELEMENT, PROJECT, TASK AREA & WORK UNIT NUMBERS Program Element No. 63431F Project No. 1227
11. CONTROLLING OFFICE NAME AND ADDRESS Defense Communications Agency 8th Street & So. Courthouse Road Arlington, VA 22204		12. REPORT DATE 30 September 1976 13. NUMBER OF PAGES 114
14. MONITORING AGENCY NAME & ADDRESS (if different from Controlling Office) Electronic Systems Division Hanscom AFB Bedford, MA 01731		15. SECURITY CLASS. (of this report) Unclassified 15a. DECLASSIFICATION DOWNGRADING SCHEDULE

16. DISTRIBUTION STATEMENT (of this Report)

Approved for public release; distribution unlimited.

17. DISTRIBUTION STATEMENT (of the abstract entered in Block 20, if different from Report)

18. SUPPLEMENTARY NOTES

None

19. KEY WORDS (Continue on reverse side if necessary and identify by block number)

adaptive nulling
multiple-beam antennas
satellite communications
antenna radiation patterns

20. ABSTRACT (Continue on reverse side if necessary and identify by block number)

This technical note discusses some of the more prominent features of an Applebaum-Howells type adaptive nulling algorithm when used in conjunction with a multiple-beam antenna operating over the earth field of view at synchronous altitude. A brief discussion of some of the basic properties of the multiple-beam antenna configuration used in the study is presented, following which some of the characteristics of the conventional LMS power minimization algorithm, such as the Applebaum-Howells type, as they apply to the multiple-beam antenna are developed. The relationship of the adapted radiation pattern to radiation pattern synthesis techniques is discussed. Next the time required for the algorithm to adapt to the steady state solution is considered. For

20. ABSTRACT (Continued)

the LMS algorithm, the dynamic range of interference power levels to be nulled sets the dynamic range of adaption times required by the adaptive algorithm. This spread in adaption times is related to the spread in the eigenvalues of the interfering-source correlation matrix defined at the receive ports. Techniques for compressing this eigenvalue spread, and hence increasing the dynamic range of the algorithm, are determined.